



This is a repository copy of *The Interpretation of Nonlinear Frequency Response Functions*.

White Rose Research Online URL for this paper:
<http://eprints.whiterose.ac.uk/78230/>

Monograph:

Billings, S.A. and Peyton Jones, J.C. (1989) *The Interpretation of Nonlinear Frequency Response Functions*. Research Report. Acse Report 375 . Dept of Automatic Control and System Engineering, University of Sheffield

Reuse

Unless indicated otherwise, fulltext items are protected by copyright with all rights reserved. The copyright exception in section 29 of the Copyright, Designs and Patents Act 1988 allows the making of a single copy solely for the purpose of non-commercial research or private study within the limits of fair dealing. The publisher or other rights-holder may allow further reproduction and re-use of this version - refer to the White Rose Research Online record for this item. Where records identify the publisher as the copyright holder, users can verify any specific terms of use on the publisher's website.

Takedown

If you consider content in White Rose Research Online to be in breach of UK law, please notify us by emailing eprints@whiterose.ac.uk including the URL of the record and the reason for the withdrawal request.



eprints@whiterose.ac.uk
<https://eprints.whiterose.ac.uk/>



THE INTERPRETATION OF NONLINEAR
FREQUENCY RESPONSE FUNCTIONS

S.A. Billings,
J.C. Peyton Jones.

Department of Control Engineering
University of Sheffield
Mappin Street
Sheffield S1 3JD
U.K.

Research Report No. 375

November 1989

November 17, 1989

THE INTERPRETATION OF NONLINEAR FREQUENCY RESPONSE FUNCTIONS

J.C. Peyton Jones, S.A. Billings.

Dept. Control Engineering, University of Sheffield, Mappin Street, Sheffield S1 3JD.

Abstract: Analytical and graphical methods of interpreting generalised frequency response functions for nonlinear systems are derived. It is shown that nonlinear phenomena can be classified into intra-kernel and inter-kernel interference and that worst case responses can be computed. The results are illustrated using several discrete and continuous time nonlinear systems.

1. Introduction

The interpretation of linear frequency response functions is founded on the close relation between analytical methods and their graphical representation. The use of Bode or Nyquist diagrams for example, is well understood and provides a powerful means of portraying system behaviour. Although several authors have introduced frequency response functions to generalise this approach to nonlinear systems, there has been no cohesive method for matching the considerable theoretical development with means to interpret such functions in physically meaningful ways.

Most nonlinear frequency domain representations have been based on the Volterra model [Volterra 1959], and numerous authors have studied the properties of this form, [Bedrosian,Rice 1971], [Bussgang,Ehrman,Graham 1974], [Chua,Ng 1979]. However the multi-dimensional nature of these generalised frequency response functions presents two immediate difficulties; firstly how to interpret frequency spaces of increasing dimension, and secondly how to relate such forms to the (uni-dimensional) system input/output spectra, [Vinh et al. 1987], [Billings,Tsang 1989].

In the present study various multi-dimensional frequency representations are interpreted in a simple graphical manner, with closely matching theoretical development. Within this framework nonlinear phenomena such as intermodulation, harmonic generation, and amplitude dependent gain/phase characteristics, may be resolved into two basic interference effects. Intra-kernel interference (which occurs within any of the Volterra kernels) is primarily nonlinear in frequency and describes the transfer of energy between spectral components. Conversely inter-kernel interference (which occurs



between each of the Volterra kernels) determines nonlinear input amplitude dependency. These mechanisms also expose the relationship between the multidimensional forms and the (uni-dimensional) system output.

Interpreting higher order frequency response functions in this way also gives insight into the structure of describing function representations, [Atherton 1975], [Gelb, Vander Velde 1968]. Indeed a worst case describing function may be obtained for a given class of inputs and order of analysis.

The paper begins in Section 2 with definitions of the Volterra series and generalised frequency response functions. Methods of interpreting the n -th order frequency domain space are given in Section 3, and illustrated with a number of examples in Section 4. Alternative frequency domain representations, which may be analytically more convenient are discussed in Section 5. Within this framework the phenomenon of intra-kernel interference is introduced in Section 6, and is used to develop an expression for the worst case n -th order output for all inputs within a given bandwidth and spectral amplitude (Section 7). The inter-kernel interference effect is introduced in Section 8, and the closely related concepts of generalised describing functions and worst case describing functions are developed in Section 9.

2. The frequency response of homogeneous functionals

A regular homogeneous functional of degree n has the property that scaling the input u by some constant c will scale the output by the same constant raised to power n . Such functionals clearly do not share the additive properties of linear systems, but are widely used in the characterisation of nonlinear systems.

Consider for example the Volterra model, [Volterra 1959], where the output may be expressed as the sum of N components $y_n(t)$,

$$y(t) = \sum_{n=1}^N y_n(t) \quad (1)$$

each of which are homogeneous of degree n . These ' n -th order outputs' are themselves defined by an extension of the familiar convolution integral of linear system theory to higher dimensions,

$$y_n(t) = \int_{-\infty}^{\infty} \cdots \int_{-\infty}^{\infty} h_n(\tau_1, \cdots, \tau_n) \prod_{i=1}^n u(t-\tau_i) d\tau_i \quad (2)$$

where the ' n -th order kernel' or ' n -th order impulse response', $h_n(\tau_1, \dots, \tau_n)$, is so called because it reduces to the linear impulse response function for the case $n = 1$.

Equation (2) may also be expressed in the frequency domain by means of the Fourier transform. Unfortunately the n -dimensional Fourier transform, which is appropriate for the right hand side of (2), cannot be applied directly to the entire equation since the left hand side $y_n(t)$ is one dimensional. It is common practice therefore to introduce the 'associated function',

$$y_n(t_1, \dots, t_n) = \int_{-\infty}^{\infty} \dots \int_{-\infty}^{\infty} h_n(\tau_1, \dots, \tau_n) \prod_{i=1}^n u(t_i - \tau_i) d\tau_i \quad (3)$$

from which the desired output $y_n(t)$ can be recovered by the restriction,

$$y_n(t) = y_n(t_1, \dots, t_n) \Big|_{t_1 = \dots = t_n = t} \quad (4)$$

The multi-dimensional Fourier transform may now be applied to both sides of equation (3) without difficulty, yielding,

$$Y_n(j\omega_1, \dots, j\omega_n) = H_n(j\omega_1, \dots, j\omega_n) \prod_{i=1}^n U(j\omega_i) \quad (5)$$

where the ' n -th order transfer function' or ' n -th order frequency response function', $H_n(j\omega_1, \dots, j\omega_n)$, is defined by,

$$H_n(j\omega_1, \dots, j\omega_n) = \int_{-\infty}^{\infty} \dots \int_{-\infty}^{\infty} h_n(\tau_1, \dots, \tau_n) e^{-j(\omega_1\tau_1 + \dots + \omega_n\tau_n)} d\tau_1 \dots d\tau_n \quad (6)$$

Notice that (6) reduces to the standard linear transfer function definition for the case $n = 1$, and that (5) would then give the familiar one dimensional relation,

$$Y(j\omega) = H(j\omega) U(j\omega) \quad (7)$$

A particular property of linear systems illustrated by this equation is that input frequencies pass independently through the system. Thus an input at a given frequency ω gives an output at the same frequency, and no energy is transferred to or from any other frequency components.

By contrast nonlinear systems may exhibit harmonics or complex intermodulations between input frequency components, and the resulting output is often highly dependent on the precise combination of frequencies applied. Unlike linear systems therefore input frequencies do not pass independently through the system, and the output may appear at some quite different frequency to the given input. The n -th order

transfer function is able to describe these interactions by means of the n frequency components which constitute its arguments.

The time and frequency domain representations (2),(5) therefore provide two equivalent system descriptions, but their relationship by means of the Fourier transform is complicated by issues of dimensionality, as illustrated in Figure 1. The frequency mapping (5) operates between two n -dimensional spaces U_{ω}, Y_{ω}^n , while the time domains U, Y_t are one dimensional. To convert between them therefore requires not only a time/frequency transformation, but also a dimensional expansion/contraction.

For the input, the change to n dimensions is fairly straightforward; the input spectrum is given by a one dimensional Fourier transform, and this is then expanded to n dimensions, within the frequency domain, by means of a simple product as illustrated by equation (5) and Figure 1. For the output, the change back to one dimension is less convenient; the associated function $y_n(t_1, \dots, t_n)$ is obtained by an n -dimensional inverse Fourier transform, while the contraction to one dimension occurs, within the time domain, by means of the restriction (4).

For these reasons it may be beneficial to combine the composite mapping $Y_{\omega}^n \rightarrow Y_t^n \rightarrow Y_t$ into a single relation,

$$\begin{aligned}
 y_n(t) &= F^{-1}[Y(\omega_1, \dots, \omega_n)] |_{t_1=\dots=t_n=t} \\
 &= \frac{1}{(2\pi)^n} \int_{-\infty}^{\infty} \dots \int_{-\infty}^{\infty} Y_n(j\omega_1, \dots, j\omega_n) e^{j(\omega_1 + \dots + \omega_n)t} d\omega_1 \dots d\omega_n
 \end{aligned} \tag{8}$$

where $F[\cdot]$ is used to denote the Fourier operator. Equation (8) coupled with (5) then shows more clearly how the input is related to the output by the n -th order transfer function, and thereby provides a basis for the interpretation of multi-dimensional frequency response plots. In Section 5 it will also be shown that equation (8) may be decomposed into the more meaningful composite mapping $Y_{\omega}^n \rightarrow Y_{\omega} \rightarrow Y_t$, (see Figure 2).

3. The input frequency domain and its interpretation

Rather than attempting to evaluate the integral (8) directly, it is worthwhile first examining the multi-dimensional frequency domain over which this integration is performed. Not only does this provide a graphical insight into many of the more familiar

analytical forms and methods, but it also gives meaning to the features of the frequency response function which lie over this domain.

For example the second order transfer function of Figure 11 exhibits several distinct ridges which lie above lines in the 2-dimensional frequency domain, (see associated contour plot). The lines may be considered as sub-domains of the overall 2-dimensional space, and each defines a relation/constraint which must be satisfied by the input frequencies if they are to excite that region.

In the following sections a number of such sub-domains are considered, and the constraints which they define are related to the input/output properties of the system so as to provide a means of interpreting the higher order frequency response functions. For ease of graphical representation the interpretations are illustrated mainly by second order examples, though they also hold for the higher order case.

3.1. Sub-domains of constant input frequency

The simplest, and perhaps most trivial sub-domains to consider are those of constant input frequency ω_{in} given by,

$$\omega_{in} = \omega_i = \text{const} \quad 1 \leq i \leq n \quad (9)$$

Clearly the ω_{in} axis is identical to any ω_i axis, and these domains are easily drawn graphically as shown for the 2nd order case in Figure 3. For this reason, and to distinguish it from other domain representations considered later, the $\omega_1, \dots, \omega_n$ domain will be called the 'input domain'.

Sub-domains of constant input frequency are closely related to the spectral components of the input $U(j\omega)$, and help to identify the points at which these interact to excite the system. For example a two tone input having spectral lines at $\pm\omega_a$ and $\pm\omega_b$ will excite a second order system as shown in Figure 4. Notice that the system is excited only at the intersection of constant input frequency sub-domains corresponding to the cartesian product $\prod U(j\omega_i)$ of equation (5). These points therefore also correspond to the particular harmonic or pairwise intermodulation of frequencies given by their frequency domain co-ordinates.

3.2. Sub-domains of constant output frequency

Just as it is important to understand which points in the multi-dimensional frequency domain are excited by constant input frequencies (Section 3.1), so it is also important to understand which points in the multi-dimensional frequency domain generate constant output frequencies. The sub-domains of constant output frequency thereby defined can then be used to expose the relationship between the multi-dimensional frequency function $Y_n(j\omega_1, \dots, j\omega_n)$ and the unidimensional output spectrum $Y_n(j\omega_{out})$, (see Section 5).

Consider first equation (8). Inspection of the exponential term shows that the output $y_n(t)$ contains a component at frequency ω_{out} given by,

$$\omega_{out} = \sum_{i=1}^n \omega_i = const \quad (10)$$

Any set of points on $Y_n(j\omega_1, \dots, j\omega_n)$ therefore, whose co-ordinates conform to (10), contribute to the same output frequency ω_{out} ; in other words (10) describes a sub-domain of constant output frequency.

Consider for example a system with an isolated quadratic nonlinearity in the input. The second order output would be of the form,

$$y_2(t) = \frac{1}{(2\pi)^2} \int_{-\infty}^{\infty} \int_{-\infty}^{\infty} Y_2(j\omega_1, j\omega_2) e^{j(\omega_1 + \omega_2)t} d\omega_1 d\omega_2 \quad (11)$$

Inspection of the exponential term, or direct application of (10), shows that the domains of constant output frequency are given by the lines,

$$\omega_{out} = \omega_1 + \omega_2 \quad (12)$$

while ω_{out} itself must increase in an orthogonal direction, namely along the line $\omega_1 = \omega_2$. These concepts are illustrated schematically in Figure 5.

Suppose then that the input was the two tone example of Section 3.1 and Figure 4. By superimposing on that figure the diagonal lines of equation (12), the output frequency corresponding to each harmonic or intermodulation is clearly seen, (Figure 6). Hence by simple graphical means a considerable insight into the nonlinear behaviour of the system is obtained.

Notice also from this example, that an output component at frequency ω_{out} is always

paired with one at $-\omega_{out}$. Indeed for any order of frequency response, it is only strictly necessary to consider the region defined by $0 \leq \omega_{out}$ since the remaining half of the multiple frequency response may be found by conjugate symmetry through the origin. This is reassuring since it implies that real inputs give real outputs.

A similar development may be applied to higher order response functions. In the 3rd order case any portion of the integrand (8) lying above the *planar* domain,

$$\omega_{out} = \omega_1 + \omega_2 + \omega_3, \quad (13)$$

again contributes to the single output frequency ω_{out} , only this time the ω_{out} 'axis' now runs (orthogonally to these domains) along the line $\omega_1 = \omega_2 = \omega_3$, as illustrated in Figure 7.

In general, although the dimensions of the constant output frequency domains increase with the order of the output (from a line to a plane and so on), the ω_{out} 'axis' will always be the line orthogonal to (10) given by,

$$\omega_1 = \dots = \omega_n \quad (14)$$

Equations (10) and (14) therefore form a useful framework with which to interpret the output properties of frequency response functions.

3.3. Sub-domains of constant frequency difference

Whilst the constant input or constant output frequency characteristics of a system are undoubtedly important, the behaviour of some nonlinear systems is dominated by the *difference* in input frequencies. This is the case when a particular intermodulation characteristic is less dependent on the absolute values of the frequencies concerned, but more dependent on their relative frequency separation. For this reason it is of interest to define sub-domains of constant frequency difference, $\Delta\omega_{ab}$, between any pair of input arguments ω_a, ω_b according to,

$$\Delta\omega_{ab} = \omega_a - \omega_b = \text{const} \quad (15)$$

Thus in the second order case such domains are given by the lines,

$$\Delta\omega_{21} = \omega_2 - \omega_1 \quad (16)$$

as shown in Figure 8. Note that a point on the line of zero difference is excited by a single frequency component, (since $\omega_1 = \omega_2$), and gives an output at twice that

frequency, (since $\omega_{out} = \omega_1 + \omega_2 = 2\omega_1$). Thus the line $\Delta\omega_{21} = 0$ corresponds to that on which harmonics of the input are generated.

The same ideas may be extended to higher orders. The second order *line* of constant frequency difference becomes a *plane* for the third order case, and so on. Note however that in these higher order cases, the pairwise definition (15) yields not one but several sub-domains of constant frequency difference. For example the third order domain has three such planes, $\Delta\omega_{32}$, $\Delta\omega_{21}$, $\Delta\omega_{13}$, , depending on which pair of frequencies are differenced. For analytical purposes it may be desirable to specify one of these only, and this may be achieved with the new definition,

$$\Delta\omega = \omega_n - \omega_{n-1} = const \quad (17)$$

Although this may appear restrictive, its use in conjunction with symmetric functions (where the order of arguments is immaterial) presents no difficulties.

3.4. Other sub-domain definitions

The sub-domains discussed in previous sections were chosen because they correspond to many of the features commonly found in multi-dimensional frequency response functions. It should be remembered however that any relation between the input arguments $\omega_1, \dots, \omega_n$ constitutes a sub-domain definition, and that input constraints in a particular situation may often have graphical as well as analytical meaning.

Consider for example a situation where the input is known to consist of a number of pure harmonics. This might arise for example in a nonlinear cascade or feedback situation where one nonlinear system generates harmonics which are fed to the input of another. Mathematically harmonic frequency components are related by the equation $\omega_i = m\omega_1$, or more specifically for the second order case,

$$\omega_2 = m\omega_1 \quad m = \frac{1}{M}, \dots, \frac{1}{2}, 1, 2, \dots, M \quad (18)$$

Thus the harmonic constraint defines lines within the second order domain of increasing gradient, representing the only points which can be excited by such an input. See Figure 9 for an illustration of these ideas. In a similar way other known relations between input frequencies may be mapped graphically, and used to indicate the regions of interest within the overall frequency domain space.

3.5. Symmetry within the input domain

Having explored various sub-domains of the input domain space, it is now worth considering the integrand $Y_n(\cdot)$ of (8) in more detail. In particular notice that this function is not unique, since permutation of any of its arguments will change the form of the function, but yield the same output $y_n(t)$ when integrated in (8). Notice also (from (5)) that this effect is experienced only through the transfer function $H_n(j\omega_1, \dots, j\omega_n)$, since (by commutativity) the order of arguments in the input $U(j\omega_i)$ is immaterial.

The use of the 'symmetric transfer' function is therefore widespread, since it alone is unique in this sense, having values which are independent of the order of its arguments. This property is obtained by summing an asymmetric function over all possible permutations of its arguments and dividing by their number, according to,

$$H_n^{sym}(j\omega_1, \dots, j\omega_n) = \frac{1}{n!} \sum_{\substack{\text{all permutations} \\ \text{of } \omega_1 \dots \omega_n}} H_n(j\omega_1, \dots, j\omega_n) \quad (19)$$

It is perhaps reassuring to note that all the permutations defined by (19) contribute to the same output frequency, since the equation $\omega_{out} = \omega_1 + \dots + \omega_n$ is unchanged by rearrangement of the ω_i . Indeed graphically speaking such functions will have reflectional symmetry about lines of equal arguments, as shown symbolically by the two dots included in the figures of this section. The appearance of the various sub-domains discussed above is therefore unchanged by the symmeterisation process.

4. Examples

4.1. Co-incident quadratic nonlinearity

Consider then a NARX model (Nonlinear Auto-Regressive, with eXogeneous inputs) [Chen,Billings 1989], with a simple input nonlinearity,

$$y(t) = 0.84u(t-1) + 0.8y(t-1) - 0.64y(t-2) - 0.04u(t-1)^2 \quad (20)$$

Such models are readily obtained for practical systems, using existing algorithms for structure detection, parameter estimation, and model validation. In this case equation (20) represents a linear digital resonator with (normalised) natural frequency $\pm\pi/3$ rads/sec, together with a quadratic nonlinear term. Indeed the first order response function is generated by the linear terms alone, see Figure 10,

$$H_1(j\omega) = \frac{0.84e^{-j\omega}}{1 - 0.8e^{-j\omega} + 0.64e^{-2j\omega}} \quad (21)$$

The second order response however is computed by a recursive 'probing' algorithm, [Peyton Jones, Billings], giving

$$H_2(j\omega_1, j\omega_2) = \frac{0.04e^{-j(\omega_1 + \omega_2)}}{1 - 0.8e^{-j(\omega_1 + \omega_2)} + 0.64e^{-2j(\omega_1 + \omega_2)}} \quad (22)$$

which is plotted in Figure 11, together with the corresponding contour diagrams. The magnitude plots exhibit three distinct ridges lying along sub-domains of constant output frequency. By graphical measurement, two of these ridges correspond to output frequencies $\omega_{out} = \omega_1 + \omega_2 = \pm\pi/3$. Thus input components whose frequencies conform to this relation transfer their energy by intermodulation to an output resonance at the system's natural frequency.

This interpretation is readily validated from the analytical form (22) whose characteristic equation is identical in form to that of (21) but with ω in the latter replaced by $(\omega_1 + \omega_2)$. Thus any inputs ω_1, ω_2 which sum to the linear resonant frequency $\pm\pi/3$, will excite the poles of the second order response and thereby generate the ridges observed in the figure. Features generated in this way are quite common in higher order frequency response plots, since it is generally the case that models of this type possess poles at output frequencies which match those of the first order characteristic equation.

There is however a third ridge which can be seen in Figure 11, corresponding to the constant output frequency domain, $\omega_{out} = \omega_1 + \omega_2 = 5\pi/3$. This output therefore occurs above the Nyquist sampling frequency of π rads/sec, and represents aliasing of some lower frequency feature.

More generally the aliasing effect causes the plots to have reflectional symmetry about the Nyquist limit $\omega_{out} = \omega_1 + \omega_2 = \pi$, so by inspection of Figure 11 the spurious ridge in this case was caused by aliasing of the one at $\omega_{out} = \pi/3$.

Similar comments can be made about the phase plots and their contour diagrams whose features are clearly aligned with the same domains of constant output frequency. Notice however the conjugate symmetry about the d.c. output sub-domain $\omega_{out} = \omega_1 + \omega_2 = 0$, which reassuringly implies that the time domain output will be real valued. In practice phase characteristics may be of considerable importance in determining interference effects between components at the same output frequency, (see Section 6).

4.2. Dynamic quadratic nonlinearity

Other features of frequency response functions may also be recognised as instances of the constant sub-domains discussed in Section 3. Consider for example the system

$$y(t) = 0.84u(t-1) + 0.8y(t-1) - 0.64y(t-2) - 0.04u(t-1)u(t-3) \quad (23)$$

where the co-incident nonlinearity $u(t-1)^2$ of the previous example has been replaced by the dynamic nonlinearity $u(t-1)u(t-3)$. The linear response remains unchanged from (21) and Figure 10. The second order response shown in Figure 12 also exhibits the same ridges as before, and the same discussion applies. An additional feature however is given by the deep gorges cutting across the second order response function along lines of constant frequency difference. By graphical measurement these gorges correspond to difference frequencies $\Delta\omega = \omega_1 - \omega_2 = \pm\pi/2, 3\pi/2$. Thus input components whose frequencies conform to this relation scarcely excite the second order kernel, and the response to this input would be purely linear.

This interpretation may also be confirmed analytically. The second order response for the modified system (23) is given by [Peyton Jones, Billings],

$$H_2(j\omega_1, j\omega_2) = \frac{0.04[e^{-j(\omega_1 + 3\omega_2)} + e^{-j(3\omega_1 + \omega_2)}]}{1 - 0.8e^{-j(\omega_1 + \omega_2)} + 0.64e^{-2j(\omega_1 + \omega_2)}} \quad (24)$$

Comparing with (22) the new features must be generated by the numerator of (24), i.e. the zeros of the system. Such zeros occur whenever the two exponential phasors cancel, i.e. whenever,

$$\omega_1 + 3\omega_2 = 3\omega_1 + \omega_2 \pm (2m+1)\pi \quad m = 0, 1, \dots \quad (25)$$

which can be rearranged to give,

$$\Delta\omega = \omega_1 - \omega_2 = \pm \frac{(2m+1)\pi}{2} \quad m = 0, 1, \dots \quad (26)$$

Thus frequencies whose difference conforms to (26), excite zeros of the second order response, and thereby generate the gorges observed in Figure 12.

4.3. Nonlinearities in continuous time

While parametric models are often used for system identification, continuous integro-differential models often result when the system is modelled from the constituent physical processes. An advantage of frequency domain interpretation however, is that it provides a common link between many model descriptions whether in discrete or

continuous time. Consider for example the continuous time model,

$$\frac{d^2y}{dt^2} + 2\zeta\omega_n \frac{dy}{dt} + \omega_n^2 y - \omega_n^2 u + 0.005\omega_n^2 y^2 = 0 \quad (27)$$

with $\omega_n = \pm 100\pi/3$, $\zeta = 0.2$. The linear terms are designed to give a continuous resonator with characteristics similar to the discrete model of equation (20). The first order response, illustrated in Figure 13, is given by,

$$H_1(j\omega) = \frac{\omega_n^2}{(j\omega)^2 + 2\zeta\omega_n(j\omega) + \omega_n^2} \quad (28)$$

In this case however the nonlinearity is in the output terms, giving the second order frequency response [Billings, Peyton Jones 1989],

$$H_2(j\omega_1, j\omega_2) = -0.005\omega_n^2 \times \frac{H_1(j\omega_1)H_1(j\omega_2)}{(j\omega_1 + j\omega_2)^2 + 2\zeta\omega_n(j\omega_1 + j\omega_2) + \omega_n^2} \quad (29)$$

which is plotted in Figure 14. As before the second order characteristic equation is identical in form to that of the linear response, but with ω in the latter replaced by the constant output frequency ($\omega_1 + \omega_2$). Thus the poles of $H_2(\cdot)$ are excited whenever $\omega_{out} = \omega_1 + \omega_2 = \pm\omega_n$, thereby generating the diagonal ridges of the second order magnitude response, (see solid lines in the contour plot). Notice that compared with the discrete case that there are no similar ridges generated by aliasing.

There are however a number of additional ridges lying along lines of constant input frequency, (see dashed lines in the contour plot). The origin of these features (and their input dependency) may be seen by the inspection of (29), where a ridge is generated whenever one of the factors $H_1(\cdot)$ is excited at the linear resonant frequency, $\pm 100\pi/3$. Local peaks may also occur whenever two or more such ridges intersect, as marked by the dots in the contour plot of Figure 14.

Such examples illustrate how an understanding of the input domain (Section 3) can prove a useful aid in the interpretation of multidimensional frequency response functions. The approach may also be extended to give representations in transformed domains whose analytic characteristics may prove advantageous.

5. Representations in transformed domains

5.1. Input/Output domain representation

The integration (8) is defined in variables of the input domain, and therefore relates closely to constant input frequency sub-domains. Interest in the output frequency response might however motivate a change of variables, so that the integration is expressed more directly in terms of the constant frequency domains defined in equation (10), and the output frequency axis given by equation (14). Making the change of variables,

$$\omega'_n = \sum_{i=1}^n \omega_i \quad (30)$$

whose inverse is,

$$\omega_n = \omega'_n - \sum_{i=1}^{n-1} \omega_i \quad (31)$$

defines what will be called the 'input/output domain' $\omega_1, \dots, \omega_{n-1}, \omega'_n$, and gives from equation (8),

$$y_n(t) = \frac{1}{(2\pi)^n} \int_{-\infty}^{\infty} \dots \int_{-\infty}^{\infty} Y_n(j\omega_1, \dots, j\omega_{n-1}, j[\omega'_n - \sum_{i=1}^{n-1} \omega_i]) e^{j\omega'_n t} d\omega_1, \dots, d\omega_{n-1}, d\omega'_n \quad (32)$$

It should not be surprising in view of the discussion Section 3.2, to note that equation (32) is in the form of an inverse Fourier transform,

$$y_n(t) = \frac{1}{(2\pi)} \int_{-\infty}^{\infty} Y_n(j\omega'_n) e^{j\omega'_n t} d\omega'_n \quad (33)$$

where

$$Y_n(j\omega'_n) = \frac{1}{(2\pi)^{n-1}} \int_{-\infty}^{\infty} \dots \int_{-\infty}^{\infty} Y_n(j\omega_1, \dots, j\omega_{n-1}, j[\omega'_n - \sum_{i=1}^{n-1} \omega_i]) d\omega_1, \dots, d\omega_{n-1} \quad (34)$$

Notice from equations (30),(10), or alternatively by direct inspection of equation (33), that sub-domains of constant output frequency are now given by,

$$\omega_{out} = \omega'_n = \text{const} \quad (35)$$

and that the output frequency axis is identical to the ω'_n axis. This is shown for the 2nd order case in Figure 15.

5.2. Output domain representation

The geometric regularity of the constant output domains, and the simplicity of equation (33), makes analysis in the input/output domain appear initially quite attractive. The form (34) is however rather cumbersome, and may be simplified if the process of changing variables is extended until the entire input domain has been transformed. Making the new change of variables,

$$\omega'_k = \sum_{i=1}^k \omega_i \quad (36)$$

whose inverse is,

$$\omega_i = \begin{cases} \omega'_i - \omega'_{i-1} & 1 < i \leq n \\ \omega'_i & i = 1 \end{cases} \quad (37)$$

defines what will be called the 'output domain' $\omega'_1, \dots, \omega'_n$, and gives from (8),

$$y_n(t) = \frac{1}{(2\pi)^n} \int_{-\infty}^{\infty} \dots \int_{-\infty}^{\infty} Y_n(j\omega'_1 j[\omega'_2 - \omega'_1], \dots, j[\omega'_n - \omega'_{n-1}]) e^{j\omega'_n t} d\omega'_1 \dots d\omega'_n \quad (38)$$

As before the n -th order output can be expressed as a simple inverse Fourier transform (33), only in this case, (39)

$$Y_n(j\omega'_n) = \frac{1}{(2\pi)^{n-1}} \int_{-\infty}^{\infty} \dots \int_{-\infty}^{\infty} Y_n(j\omega'_1 j[\omega'_2 - \omega'_1], \dots, j[\omega'_n - \omega'_{n-1}]) d\omega'_1 \dots d\omega'_{n-1}$$

Notice with reference to Section 2, that equations (33),(39) decompose the single mapping $Y_\omega^n \rightarrow Y_t$ given by (8), into the composite $Y_\omega^n \rightarrow Y_\omega \rightarrow Y_t$, (see Figure 2). By comparison with the alternative composite Figure 1, this represents a considerable advantage, for not only does it dispense with the artificiality of the associated function, but it introduces the more meaningful spectrum $Y(j\omega)$.

Not unnaturally the sub-domains of constant output frequency remain as shown in Figure 15, with the output frequency axis identical to the ω' axis. Indeed for the second order case equations (34),(39) are identical. However the difference between the input/output and output domains becomes apparent for higher orders.

This difference is best illustrated by considering the representation of sub-domains of constant input frequency in the newly defined forms. In the input/output domain these are largely unaltered, and only the n -th input frequency domain is changed according to (31). In the output domain however all (bar the first) sub-domains of constant input

frequency are changed according to the relation (37).

Although the second order example does not highlight this difference, it does serve to show how a sub-domain of constant input frequency is transformed by the change of variables (31) or (37), - that is (see Figure 16),

$$\omega_2 = \omega'_2 - \omega'_1 = \text{const} \quad (40)$$

Note in comparison with Figure 3, that it is more difficult to visualise domains of constant input frequency within the output frequency domain, than it is to visualise domains of constant output frequency within the input frequency domain.

For completeness consider also how sub-domains of constant frequency difference map into the output domain. Substituting for ω_n, ω_{n-1} in equation (17) gives from equation (37) (for the case $n = 2$),

$$\Delta\omega = \omega'_2 - 2\omega'_1 = \text{const} \quad (41)$$

and these second order sub-domains are shown in Figure 17. Notice again that the transformation has adversely affected the geometric appearance of the $\Delta\omega$ sub-domains.

Thus the output domain representation may sometimes present some analytical advantages, and certainly makes sub-domains of constant output frequency appear more regular. However this is achieved at the expense of other sub-domains of interest, whose geometric representation is more difficult to visualise in the new form. For this reason, and for reasons discussed under 'Symmetry' below, the output domain representation will be used in analytical arguments, but these will be illustrated in input domain graphical form.

5.3. Other domain representations

The process of changing variables described above may be used in a similar way to define many other domain representations. For example a 'difference' domain, $\omega''_1, \dots, \omega''_n$, which caused sub-domains of constant frequency difference to appear more regular, could be defined as,

$$\omega''_i = \begin{cases} \omega_i - \omega_{i-1} & 1 < i \leq n \\ \omega_i & i = 1 \end{cases} \quad (42)$$

Unfortunately transformations such as equation (42) possess similar difficulties of visual interpretation to those experienced within the output domain, but may not yield analytical advantages of the latter. Meanwhile other transformations, such as a simple rotation, may preserve visual features but complicate analysis by introducing non-unity Jacobians.

5.4. Symmetry within transformed domains

The process of changing variables described above implicitly defines new frequency response functions in each domain. Thus for example,

$$G_n^{out}(j\omega'_1, \dots, j\omega'_n) = G_n(j\omega'_1 j[\omega'_2 - \omega'_1], \dots, j[\omega'_n - \omega'_{n-1}]) \quad (43)$$

defines a new function in the output domain. Indeed the 'regular' transfer function of Mitzel et al [Mitzel, Clancy, Rugh 1979] is derived (from their 'triangular' function) in such a way.

Such functions may be unique in the sense that they were calculated by transformation of an input domain symmetric function, but not in the symmetric sense discussed in Section 3.4. Indeed an input domain symmetric function transformed for example to the output domain, has its symmetry warped by the new co-ordinate axes,

(note the symbolic dots included in Figure 17 which are no longer symmetric about the line of equal arguments). However symmetrisation analogous to (19) may be applied directly in the new domain, giving functions whose values are once more independent of the order of their (transformed) arguments.

As expected functions symmeterised in this way become analytically more amenable. For example it is then possible to rewrite (33) for any ω'_i , and any axis could be used as the ω_{out} axis. However graphical visualisation may become more complicated; for example symmeterisation of the output domain introduces reflectional symmetry about lines of equal arguments, so that domains of constant frequency difference now appear as shown in Figure 18, (compare Figure 17).

6. Intra-kernel interference

Having identified those points in the frequency domain which contribute to the same output frequency (Section 3.2), it is also important to understand how these (multi-dimensional) components combine and collapse to form a uni-dimensional output spectrum. Mathematically this process is given by equation (39), which shows that the final output $Y(j\omega)$ at any given frequency results from an integration across the corresponding constant output frequency sub-domain.

Consider for example the two tone case of Figure 6, (illustrated in the input domain). Since the system is excited only at a few discrete points, the integration (39) reduces to a simple summation across each diagonal sub-domain of constant output frequency. Thus the d.c output results from a summation of four contributions, the intermodulation output $\omega_a - \omega_b$ from a summation of two, and so on. Notice however that each contribution is a complex or vector quantity having magnitude and phase. The integration/summation therefore consists of a vector addition of components which may act constructively or destructively upon one another. Thus equation (39) is highly significant, for it describes an interference effect between output components which will be termed 'intra-kernel interference'.

To illustrate this phenomenon consider again the example system 4.3, with a continuous time quadratic nonlinearity. Suppose the system were excited in such a way as to produce two intermodulations, marked a, b , within the same constant output frequency sub-domain, as shown on the contour plots of Figure 14. The gain/phase response at each point may be represented by a phasor, so that their combined contribution to the output at that frequency is given by the vector diagram Figure 19(a). Notice that the two contributions are broadly in phase, so that the phasors a, b combine constructively giving a large resultant $R_{a,b}$.

Suppose now that the input is changed so that the system is no longer excited at point b , but at another point c (still within the same constant output frequency sub-domain). In this case the vector combination of a and c are not so well aligned, causing destructive interference and a smaller resultant output $R_{a,c}$, shown in Figure 19(b).

Particularly dramatic examples of constructive/destructive intra-kernel interference may also be seen by inspection of Figures 11,12. In the former case, all points within a given output domain are perfectly in phase, giving the maximum superposition of the

output components. In the latter case however the phase is reversed as the domain of constant output frequency is traversed by one of the gorges in the figure. Points either side of these gorges are therefore in perfect anti-phase, giving the maximum cancellation between any such output contributions.

Such examples illustrate that intra-kernel interference can have a very profound effect on the final output, and in particular that it may be misleading to interpret the magnitude response alone without regard to the phase of those points of interest.

When more input frequencies are involved the situation becomes more complicated to visualise, but the same principle underlying equation (39) applies. Consider for example a system excited by white noise of variance A . The input therefore has a flat spectrum of amplitude A , and excites every point of the transfer function into the response. Indeed using equation (5) the output spectrum (39) may be rewritten,

$$Y_n(j\omega) = \frac{A^n}{(2\pi)^{n-1}} \int_{-\infty}^{\infty} \cdots \int_{-\infty}^{\infty} H_n(j\omega'_1, j[\omega'_2 - \omega'_1], \cdots, j[\omega'_n - \omega'_{n-1}]) d\omega'_1 \cdots d\omega'_{n-1} \quad (44)$$

showing again how the multi-dimensional response is collapsed down to a one dimensional output spectrum. In the process of this complex/vector integration all the points within a given sub-domain of constant output frequency interact in the manner described above. Depending on the exact form of $H_n(\cdot)$ they may act constructively, but equally it is possible that they may act destructively, with one intermodulation cancelling the effect of another. The white noise response therefore does not necessarily give the worst case output, and cannot guarantee that every nonlinear mode reaches the final output. However the concept of a (unidimensional) worst case response could be useful, and is further developed below.

7. Worst case n-th order output response

The discussion of Section 6 illustrates how it is possible to obtain a unidimensional n -th order output response for a nonlinear system, but only for a particular known input or combination of input frequencies. Indeed it is for this reason that a nonlinear transfer function is multi-dimensional in frequency so that any possible input combination may be accommodated.

However in spite of the interpretations given in this paper, the multi-dimensional form

is not easy to assimilate, particularly for higher orders. In addition there are many cases where the precise form of the input is not known. Another approach therefore might be to sacrifice the detail of such descriptions for the clarity of the unidimensional response, and introduce instead bounds of uncertainty to accommodate a *range* of possible inputs. Of course if an interesting feature were detected in this 'worst case n -th order output', then the analyst could examine it in more detail by reverting to the multidimensional form.

A suitable class of inputs to consider might be defined as falling within a frequency bandwidth ω_b and spectral amplitude range $\leq A$. The worst case output can then be obtained in a manner similar to that already described for white noise, only in this case every point is forced to act constructively by integrating only the modulus of the frequency response, and assuming that all points are in phase, (45)

$$Y_n^{worst}(\omega) = \frac{A^n}{(2\pi)^{n-1}} \int \cdots \int |H_n(j\omega'_1 j[\omega'_2 - \omega'_1], \cdots, j[\omega'_n - \omega'_{n-1}])| d\omega'_1 \cdots d\omega'_{n-1}$$

Thus the worst case input is similar to white noise in the sense that it excites every point of the n -th order transfer function into the response, but it has the additional property that its phase brings all these contributions in line so that they all act constructively. The resulting output spectrum then has a magnitude bound given by equation (45) and arbitrary phase.

Finally some consideration must be given to the bounds of integration, for although the input is bounded by ω_b , equation (45) is expressed in the output domain $\omega'_1 \cdots \omega'_n$. The new limits may be found by applying the input constraint on equations (36),(37), giving

$$|\omega'_i| \leq i\omega_b \quad 1 \leq i \leq n \quad (46)$$

$$\omega_b \geq \begin{cases} |\omega'_i - \omega'_{i-1}| & 1 < i \leq n \\ |\omega'_i| & i = 1 \end{cases} \quad (47)$$

Since the output frequency ω'_n is fixed, equation (47) may be rewritten with shifted indices and rearranged to give,

$$|\omega'_i| \geq |\omega'_{i+1}| - \omega_b \quad 1 \leq i \leq n-1 \quad (48)$$

Using (46),(48) equation (45) may be given more explicitly as, (49)

$$Y_n^{worst}(\omega) = \frac{A^n}{(2\pi)^{n-1}} \int_{\min\{i\omega_b, (\omega_{i+1} + \omega_b)\}}^{\max\{-i\omega_b, (\omega_{i+1} - \omega_b)\}} \cdots \int |H_n(j\omega'_1 j[\omega'_2 - \omega'_1], \cdots, j[\omega'_n - \omega'_{n-1}])| d\omega'_1 \cdots d\omega'_{n-1}$$

which using (43) may also be written,

$$Y_n^{worst}(\omega) = \frac{A^n}{(2\pi)^{n-1}} \int_{\min\{i\omega_b(\omega_{i+1}+\omega_b)\}}^{\max\{-i\omega_b(\omega_{i+1}-\omega_b)\}} \cdots \int |H_n^{out}(j\omega'_1, \cdots, j\omega'_n)| d\omega'_1 \cdots d\omega'_{n-1} \quad (50)$$

7.1. Examples

Consider again the continuous time nonlinear system of equation (27) excited by any input within the bandwidth $\omega_b = 100\pi$, and spectral amplitude range $A \leq 0.8$. The worst case second order output spectrum for this class of inputs may be found by integrating $|H_2(\cdot)|$ along sub-domains of constant output frequency according to equations (49), or (50). Performing this integration numerically collapses the second order transfer function of Figure 14 to the magnitude bound shown in Figure 20, while the phase is arbitrary. This form, being one dimensional in frequency, is easier to comprehend, but still retains some of the dominant features of its multidimensional counterpart. For example the resonance of Figure 20 corresponds to the diagonal ridges of Figure 14, which are in turn generated by the poles of the second order transfer function as discussed in Section 4.3.

The same approach may also be applied to higher order responses which otherwise have no graphical representation. Consider for example the third order transfer function of equation (27) which is given by,

$$H_2(j\omega_1, j\omega_2, j\omega_3) = \frac{-0.005\omega_n^2}{2} \times \frac{H_1(j\omega_1)H_2(j\omega_2, j\omega_3) + 2H_1(j\omega_2)H_2(j\omega_1, j\omega_3) + H_1(j\omega_3)H_2(j\omega_1, j\omega_2)}{(j\omega_1 + j\omega_2 + j\omega_3)^2 + 2\zeta\omega_n(j\omega_1 + j\omega_2 + j\omega_3) + \omega_n^2} \quad (51)$$

The response, having three dimensions, cannot easily be plotted graphically. However the third order worst case output spectrum can be obtained by integrating $|H_3(\cdot)|$ over all the planar sub-domains of constant output frequency within the input bandwidth according to equations (49), or (50). The resultant magnitude bound is shown in Figure 21.

8. Inter-kernel interference

Having examined the factors affecting the n -th order output response, it now remains to see how the response of different orders combine together.

The total output response at any given frequency may be given by the Fourier transform of equation (1),

$$Y(j\omega) = \sum_{n=1}^{\infty} Y_n(j\omega) \quad (52)$$

and is clearly dependent on the n -th order responses. To separate these two discussions therefore, it will be assumed that the input spectrum remains unchanged, except perhaps for a pure change in scale A . Each n -th order output $Y_n(j\omega)$, being homogeneous, is therefore also constant apart from a change in the scale of A^n . Equation (52) then becomes,

$$Y(A, j\omega) = \sum_{n=1}^N A^n Y_n(j\omega) \quad (53)$$

where the $Y_n(j\omega)$ may be considered as some constant set of spectra which have been pre-determined according to equations (34) or (39). The summation of equation (53), which combines the contributions from each order, can then be considered in relative isolation.

Firstly it is important to note that equation (53) is one-dimensional, and that the final output at frequency ω is obtained only from components in each n -th order output at this frequency. Unlike intra-kernel effects therefore, this combination of components from different kernels does not involve any intermodulation or transfer of energy between frequencies.

However it should also be noted that the contributions from each kernel at a given frequency, being complex (phasor) quantities, may act constructively or destructively on one another in the summation (53). This equation is therefore highly significant, for it describes an interference effect between output components from different orders which will be called 'inter-kernel interference'.

To demonstrate this phenomenon consider the case where the n -th order responses at a given frequency ω_a are those given in Figure 22(a) — (These values have been chosen for clarity of illustration, and do not correspond to any of the examples in Section 4).

Each response, having magnitude and phase, may be represented by a phasor, so that their summation can be depicted by the vector diagram, Figure 22(a). In this case the original magnitude of the linear frequency response $Y_1(j\omega)$ is increased by the phasor addition of higher order contributions, and the inter-kernel interference effect may be classified as 'gain expansion'. At another frequency ω_b , the same system may have the n -th order responses shown in Figure 22(b). In this case the magnitude of the linear frequency response $Y_1(j\omega)$ is decreased by the addition of the nonlinear components, giving a destructive interference effect or 'gain compression'.

As well as altering the magnitude of the linear response, inter-kernel interference also modifies the phase. For example the nonlinear contributions of Figure 22(a) retard the phase of the resultant relative to that of $Y_1(j\omega)$, while those of Figure 22(b) cause phase advance. Such phase effects should not be overlooked, particularly in control applications where the phase crossover point can be vital in the design of stable controllers. Notice also that phase advancement/retardation and gain expansion/compression can occur in any combination since the resultant output phasor may lie in any of the areas shown in Figure 23.

Another property of inter-kernel interference is the dependence on the input amplitude A . By inspection of equation (53) a value of $A < 1$ gives a decreasing weight to the higher order output response contributions, while values of $A > 1$ increase their significance. This is in agreement with the observation that nonlinear systems may appear almost linear at low input amplitudes, but become increasingly nonlinear in their behaviour as the input amplitude is increased.

Such amplitude effects may again be illustrated using phasor representations. If for example the input amplitude for the vector diagrams of Figure 22 were doubled, the linear output $Y_1(j\omega)$ doubles, the second order phasor $Y_2(j\omega)$ quadruples, and so on. The increased input amplitude results in an unequal scaling of the phasor contributions of each n -th order output, and considerably modifies the shape of each diagram, as shown (half scale) in Figure 24(a),(b). Notice that the change in input amplitude was sufficient to drive the resultant output at frequency ω_a from an area of gain expansion into one of gain compression, (compare Figures 22(a),24(a)). Indeed high amplitude gain compression is fairly common, and corresponds to saturation of the system.

9. Generalised describing functions

The output response resulting from inter-kernel interference has close links with the describing function approach to nonlinear systems analysis. The latter is a quasi-linear (but amplitude dependent) transfer function relating input and output components at the same frequency,

$$N(A, j\omega) = \frac{Y(A, j\omega)}{A U(j\omega)} \quad (54)$$

Equation (54) might suggest that input frequencies pass independently through the system, whereas in reality there may be considerable interaction through intermodulations and intra-kernel interference. For this reason the describing function definition is restricted to a specific input waveform such as, for example, a single sinusoid, and the approach is rarely extended beyond the two tone case. More generally however, equations (53),(54) may be combined to give,

$$N(A, j\omega) = \frac{1}{U(j\omega)} \sum_{n=1}^N A^{n-1} Y_n(j\omega) \quad (55)$$

where $N(A, j\omega)$ is considered to be undefined at any frequencies $U(j\omega) = 0$. Note that the spectrum $Y_n(j\omega)$ is given by the intra-kernel equations (34) or (39), and therefore accomodates any given frequency combination.

Expanding the first term of equation (55) yields,

$$N(A, j\omega) = H_1(j\omega) + \frac{1}{U(j\omega)} \sum_{n=2}^N A^{n-1} Y_n(j\omega) \quad (56)$$

Thus the describing function is given by the linear response, whose gain and phase are modified by the inter-kernel interference terms of higher order.

While equation (56) may be illustrated by the phasor diagrams similar to those of the previous section, the describing function representation enables input and output to be related more directly. For example the amplitude dependence of gain compression/expansion at a given frequency may be illustrated using a 'gain response curve' as shown in Figure 25(a). If the system were in fact linear, then the input/output amplitudes would be related by the dotted straight line of the figure, whose gradient is indeed the linear gain $|H_1(j\omega)|$. Nonlinear components modify this response, giving an augmented output (gain expansion) at points above the dotted line, or a decreased output (gain compression) below it. The two marked points correspond to the phasor plots Figures 22(a),24(a), and demonstrate how these curves may be obtained by evaluating

equation (53) at different input amplitudes.

The effect of amplitude on phase advancement/retardation may also be depicted in a similar manner by means of a 'phase response curve' as shown in Figure 25(b). In this case the linear phase is independent of input amplitude, giving the horizontal dotted line of the figure. However inter-kernel interference from nonlinear components in the output can cause phase advancement, raising the curve above the dotted linear response, or retardation which lowers it. Again the marked points on the figure correspond to the phasor plots Figures 22(a),24(a) which illustrate the interference mechanism at any given amplitude.

9.1. Worst case describing functions

While the expression (56) provides a means to derive a describing function for any given input, it then remains specific to that input. An alternative might be to derive a describing function with bounds of uncertainty to accommodate a whole class of inputs. The basis of this approach lies in the worst case n -th order output response function of Section 7, and the describing function equation (56). A worst case describing function may then be defined as,

$$N(A,j\omega)^{worst} = H_1(j\omega) + \sum_{n=2}^N A^{n-1} Y_n^{worst}(\omega) \quad (57)$$

Note that $Y_n^{worst}(\omega)$ represents a magnitude bound with arbitrary phase, and division by the unity amplitude spectrum $U(j\omega)$ in equation (56) is therefore immaterial in this case.

The lack of phase information also makes it impossible to distinguish between gain compression or expansion, or between phase advancement or retardation. Instead the worst case describing function gives circles of uncertainty of radius $\Delta H(\omega)$,

$$\Delta H(\omega) = \sum_{n=2}^N \Delta H_n(\omega) = \sum_{n=2}^N A^{n-1} Y_n^{worst}(\omega) \quad (58)$$

which are imposed on the linear response as shown in the phasor plot Figure 26. Notice that the maximum phase uncertainty $\Delta\phi$, introduced by the nonlinearities, depends on the magnitude of the linear response, since by simple trigonometry from the figure,

$$\Delta\phi \equiv \arctan \left[\frac{\Delta H(\omega)}{|H_1(j\omega)|} \right] \quad (59)$$

The gain and phase uncertainties, $\Delta H(\omega), \Delta\phi$, have the same amplitude dependence as any describing function, i.e. doubling the input amplitude, for example, doubles the second order uncertainty, quadruples that of the third order, and so on. This effect may be depicted using gain or phase response curves similar to those of the previous section, only in this case the curves themselves are replaced by bands of uncertainty as shown in Figure 27. However the existence of a well defined input at all frequencies within the specified bandwidth ensures that equation (57) is also well defined at all frequencies of interest. Thus the gain and phase response plots, which relate amplitude dependence at a constant input frequency, may be complemented by worst case Bode or Nyquist plots across all the frequencies of the bandwidth, but at constant amplitude.

9.2. Examples

Consider once again the continuous time nonlinear system of equation (27) excited by any input within the bandwidth $\omega_b = 100\pi$, and spectral amplitude range $A \leq 0.8$. The worst case second and third order output spectra shown in Figures 20,21 may now be combined with the linear response to give a worst case describing function according to equation (57), with analysis truncated above third order. The result is plotted in Figure 28, with the familiar linear transfer function shown in solid line, surrounded by bands of uncertainty $\Delta H(\omega), \Delta\phi$ shown in dotted form.

The bands are quite wide and may in practice be overly pessimistic. Nevertheless they do provide a useful overview of the system behaviour. For example the major uncertainty in this case is at low frequencies, and the dominant resonance still occurs at the linear resonant frequency. The gain and phase margins also have been seriously encroached by the system nonlinearities, though for this (truncated) analysis the system remains stable. Notice also that if more information were available concerning the system inputs, it might be possible to contract the bands of uncertainty by restricting the class of inputs considered.

10. Conclusions

The n -dimensional frequency domain has been interpreted by defining sub-domains which relate directly to the system input/output behaviour. Based on these forms various alternative domain representations which stress system output properties have also been considered. The interpretation of the n -dimensional frequency space gives meaning to the generalised frequency response functions of nonlinear systems, and exposes the relationship between the (uni-dimensional) input/output spectrum and the multi-dimensional model form. In particular nonlinear effects may be divided into those which are intra-kernal and primarily frequency dependent, and those which inter-kernel and primarily amplitude dependent. These mechanisms which reduce dimensionality give insight into describing function analysis, and also enable the 'worst case' response for a specified class of inputs and order of analysis to be determined. In some cases the latter may be overly pessimistic but can still provide a useful overview of the system behaviour.

References

- ATHERTON, D.P., (1975). *Nonlinear Control Engineering*, Van Nostrand Reinhold, London.
- BEDROSIAN, E. AND RICE, S.O., (1971). "The Output Properties of Volterra Systems (Nonlinear Systems with Memory) Driven by Harmonic and Gaussian Inputs," *Proc. IEEE*, vol. 59, pp. 1688-1707.
- BILLINGS, S.A. AND PEYTON JONES, J.C. (1989). "Mapping Nonlinear Integro-Differential Equations Into the Frequency Domain," Report No. 366.
- BILLINGS, S.A. AND TSANG, K.M., (1989). "Spectral Analysis for Nonlinear Systems. Part II - Interpretation of Nonlinear Frequency Response Functions," *Mechanical Systems and Signal Processing*, vol. 3, no. 4, pp. 341-359.
- BUSSGANG, J.J., EHRMAN, L., AND GRAHAM, J.W., (1974). "Analysis of Nonlinear Systems with Multiple Inputs," *Proc. IEEE*, vol. 62, pp. 1088-1119.
- CHEN, S. AND BILLINGS, S.A., (1989). "Representations of Nonlinear Systems: The NARMAX Model," *Int J. Control*, vol. 49, pp. 1013-1032.
- CHUA, L.O. AND NG, C.Y., (1979). "Frequency domain analysis of nonlinear systems: general theory," *IEE Journal Electronic Circuits and Systems*, vol. 3, no. 4, pp. 165-185.
- CHUA, L.O. AND NG, C.Y., (1979). "Frequency domain analysis of nonlinear systems: formulation of transfer functions," *IEE Journal Electronic Circuits and Systems*, vol. 3, no. 6, pp. 257-269.
- GELB, A. AND VANDER VELDE, W.E., (1968). *Multiple-Input Describing Functions and Nonlinear System Design*, McGraw-Hill, New York.
- MITZEL, G., CLANCY, S., AND RUGH, W., (1979). "On transfer function representations for homogeneous nonlinear systems," *IEEE Trans. on Automatic Control*, vol. AC-24, pp. 242-249.
- PEYTON JONES, J.C. AND BILLINGS, S.A., "A Recursive Algorithm for Computing the Frequency Response of a Class of Nonlinear Difference Equation Models," *Int J. Control (to appear)*.
- VINH, T., CHOUYCHAI, T., LIU, H., AND DIOUDER, M., (1987). *Second order transfer function: computation and physical interpretation*, 5th IMAC, London.
- VOLTERRA, V., (1959). *Theory of functionals and of integral and integrodifferential equations*, Dover, New York.

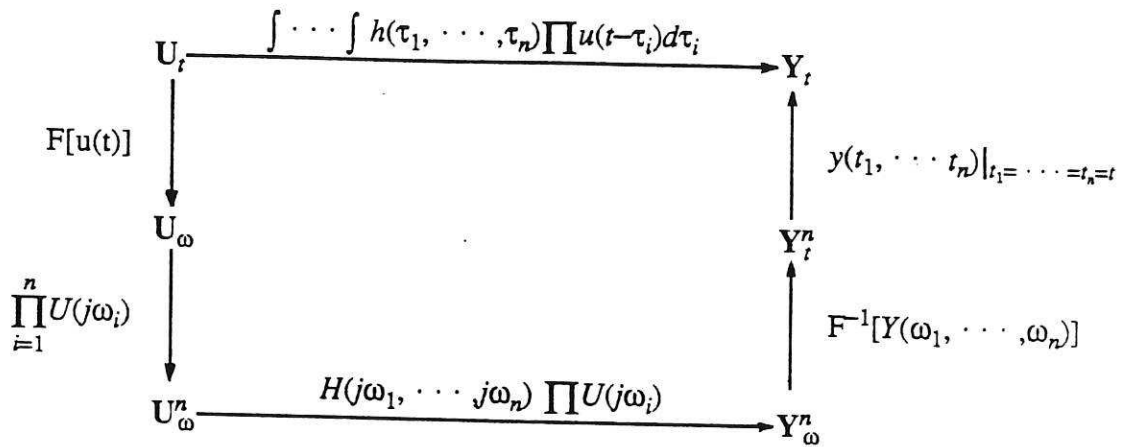


Figure 1

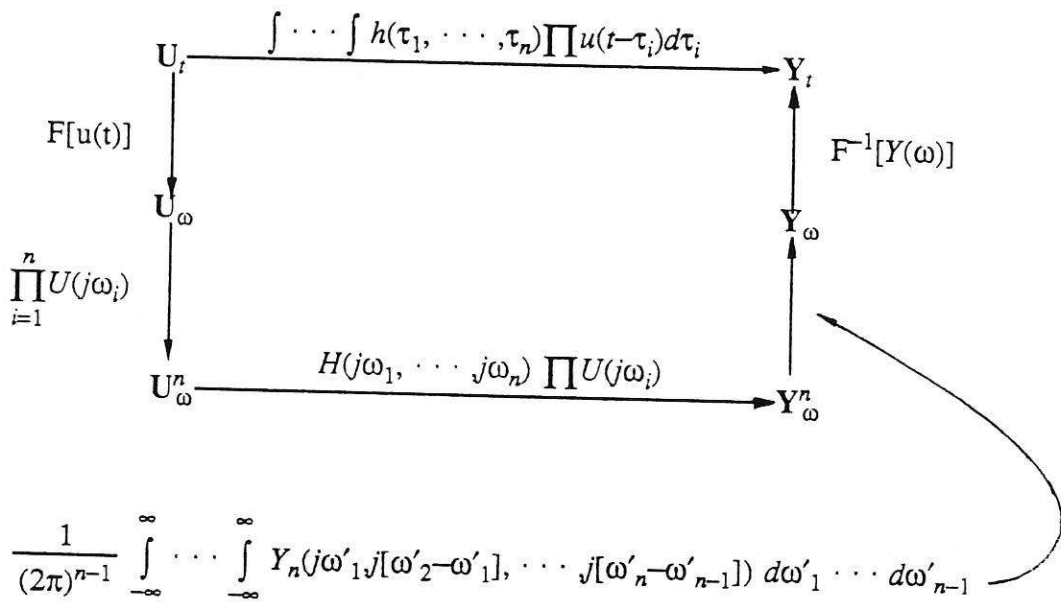


Figure 2

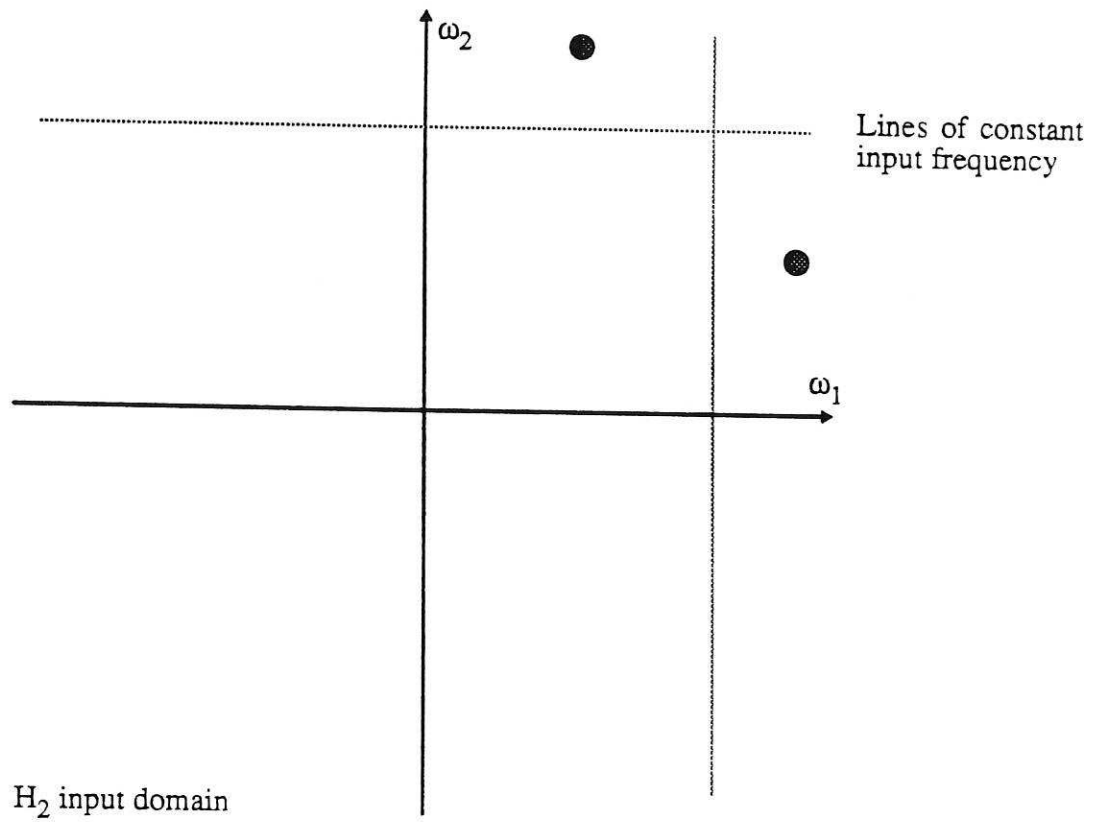


Fig 3 Constant input frequency sub-domains

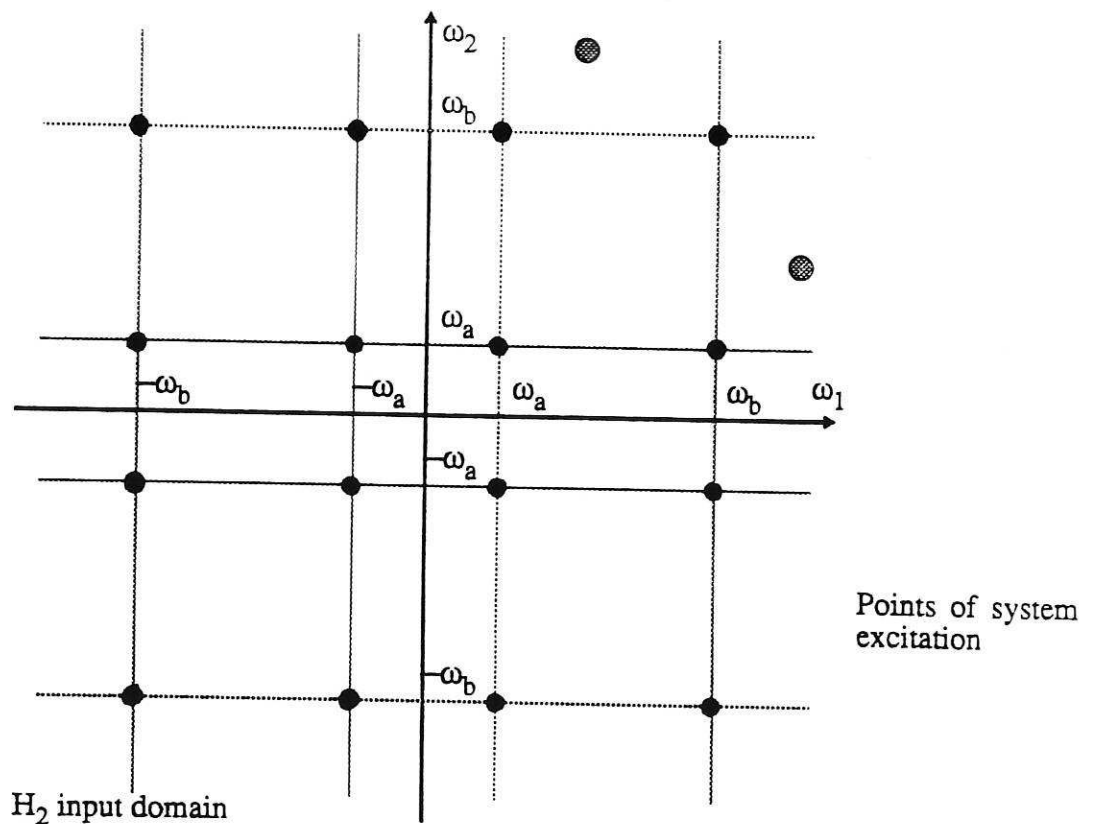


Fig 4 Points of excitation for two tone input

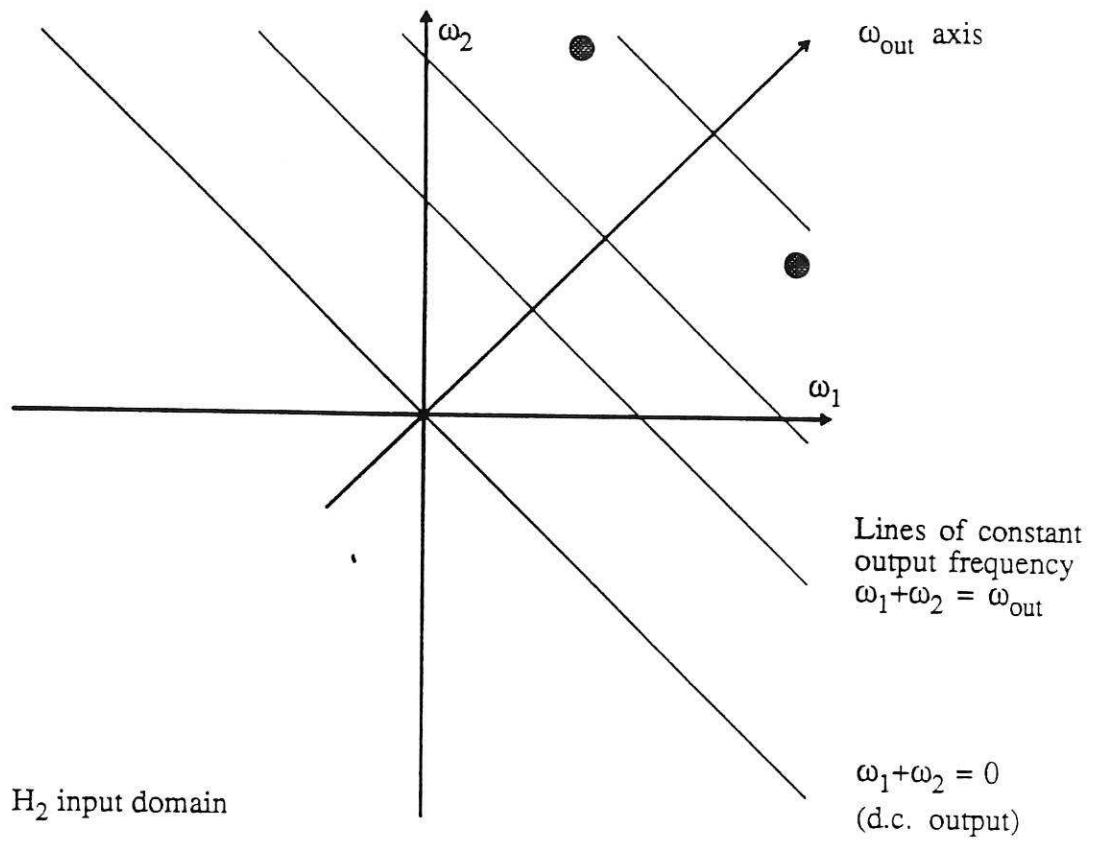


Fig 5 Constant output frequency sub-domains

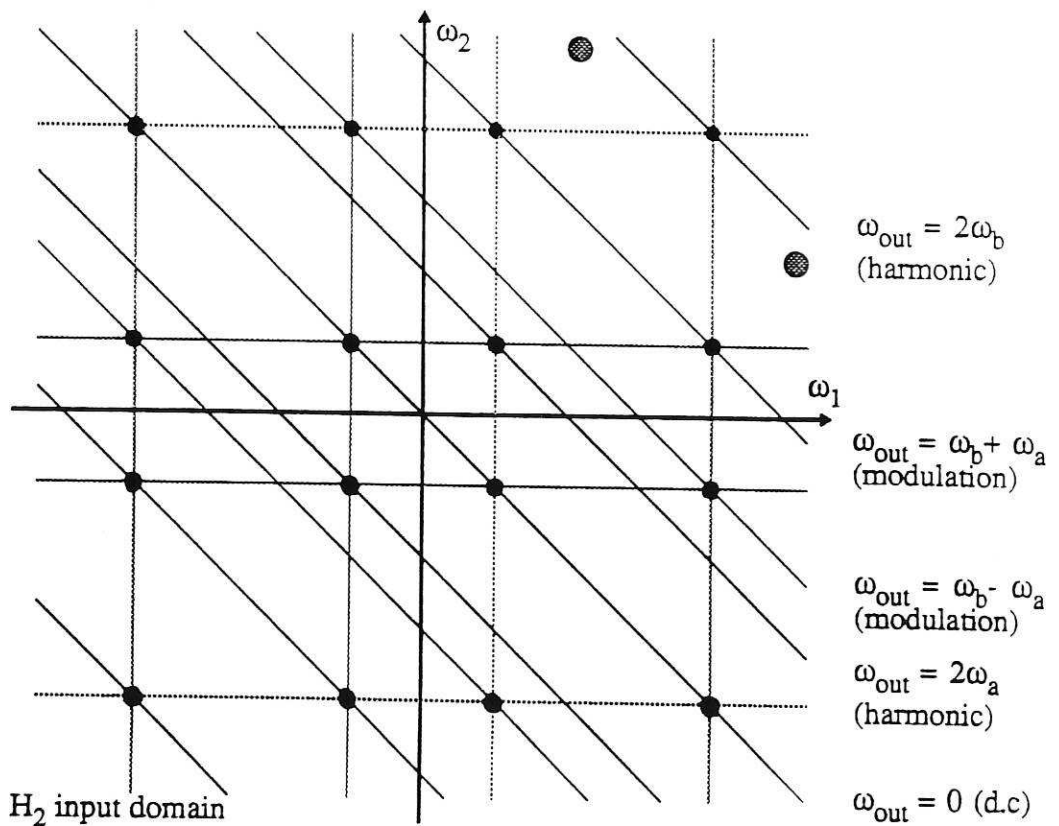
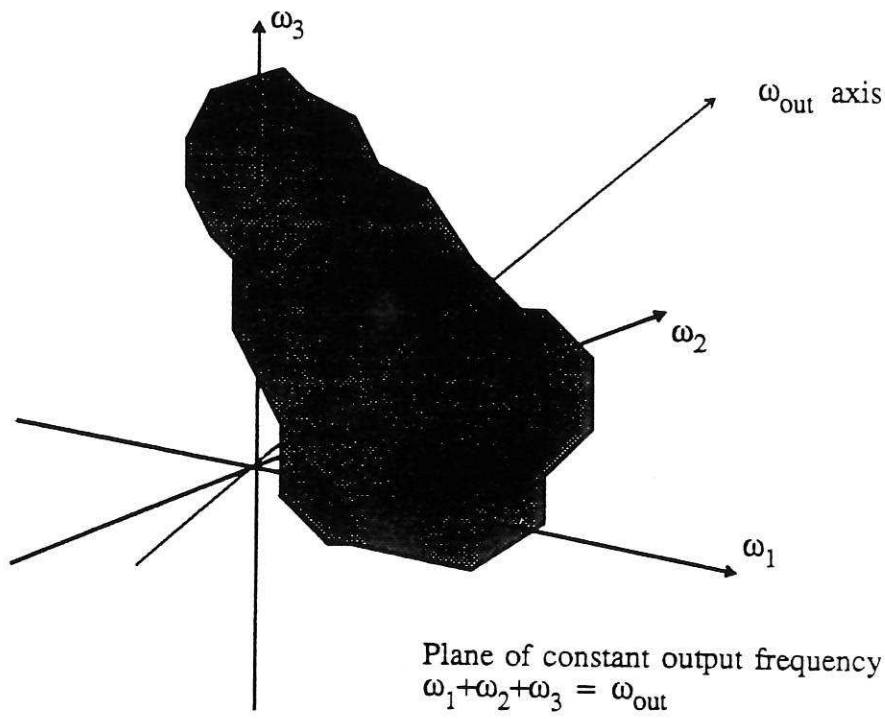


Fig 6 Output frequencies generated by two tone input



H₃ input domain

Fig 7 Constant output frequency sub-domain in H₃

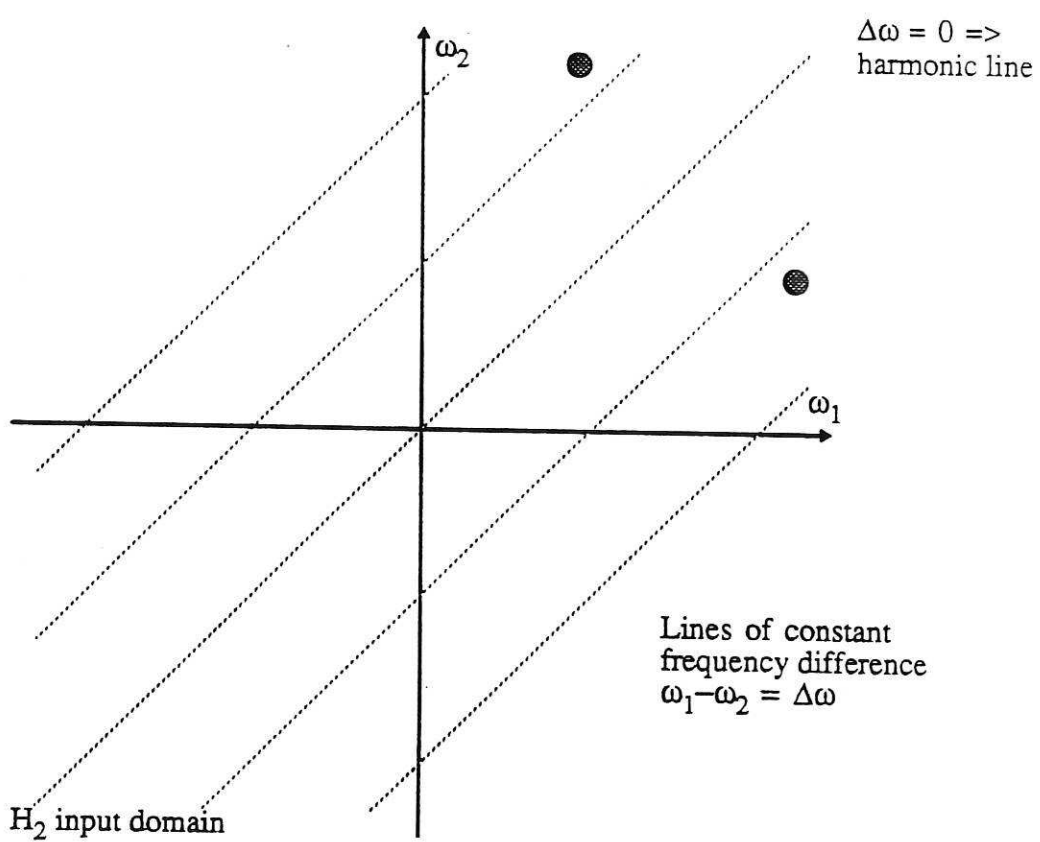


Fig 8 Constant difference frequency sub-domain

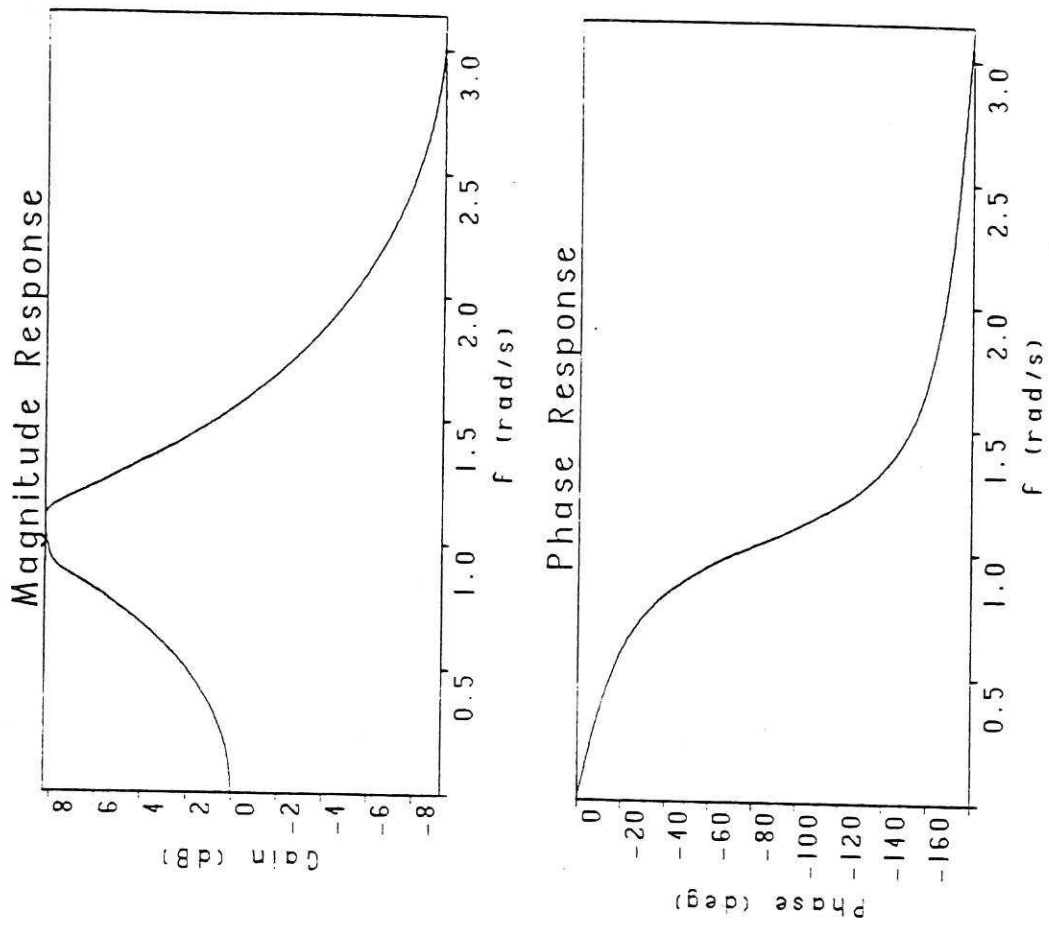


Fig 10. Linear response

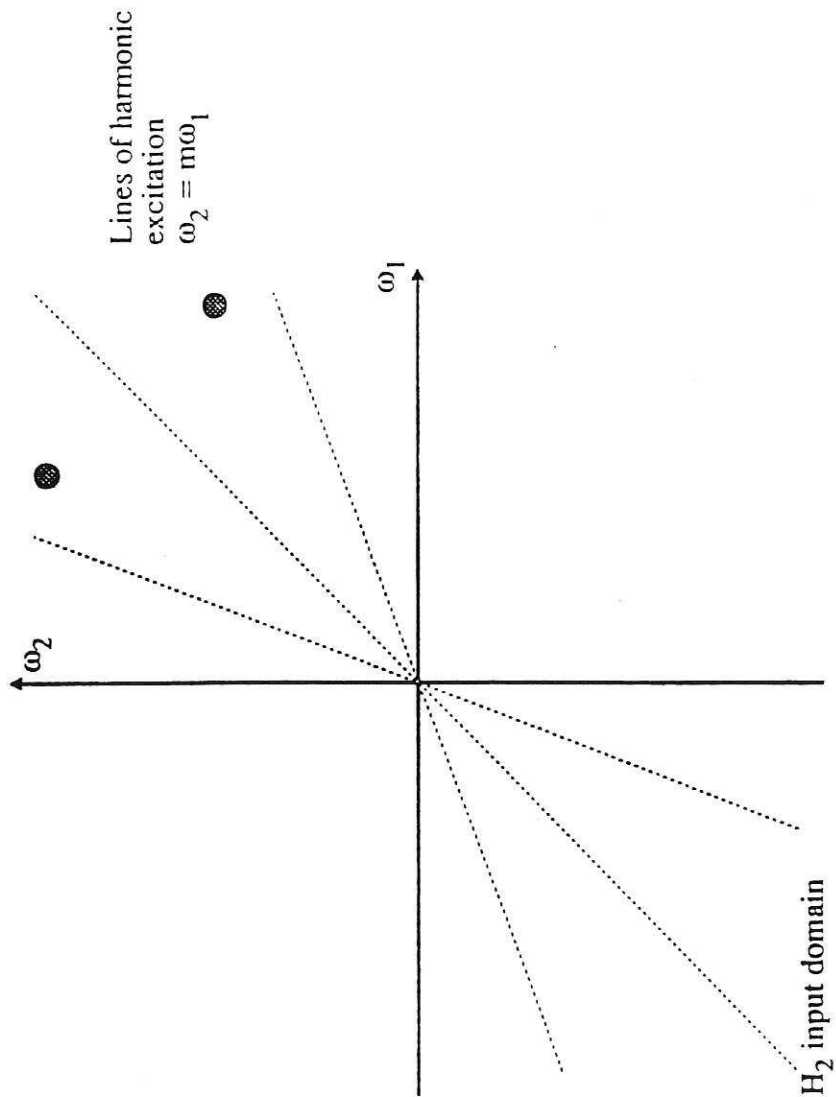


Fig 9 Harmonic excitation sub-domains

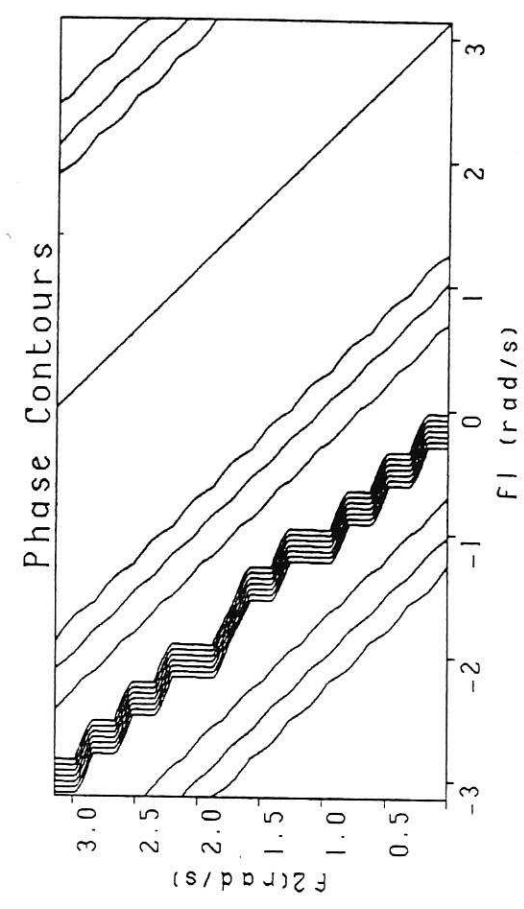
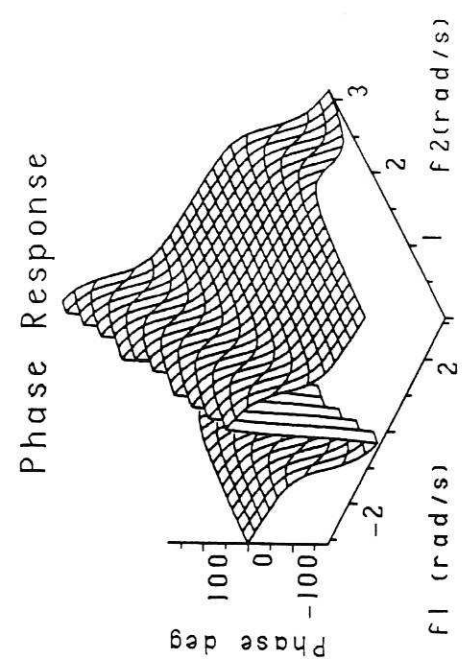
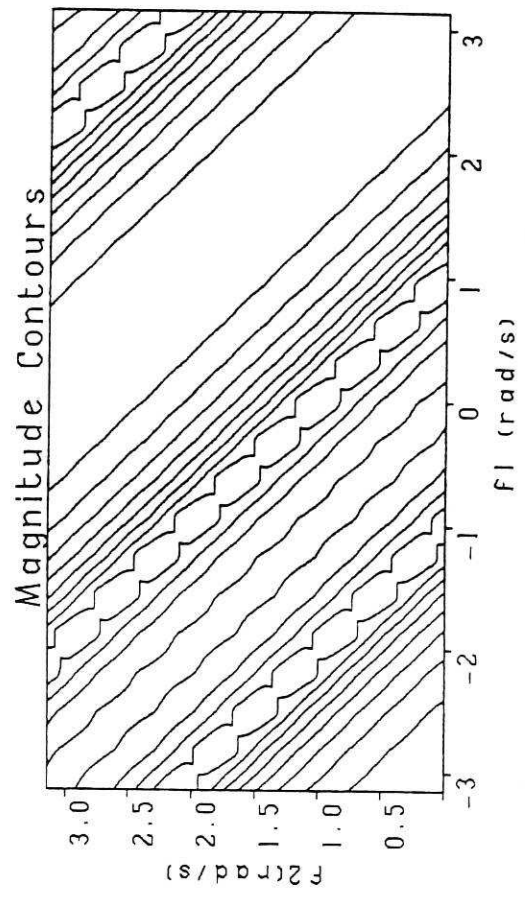
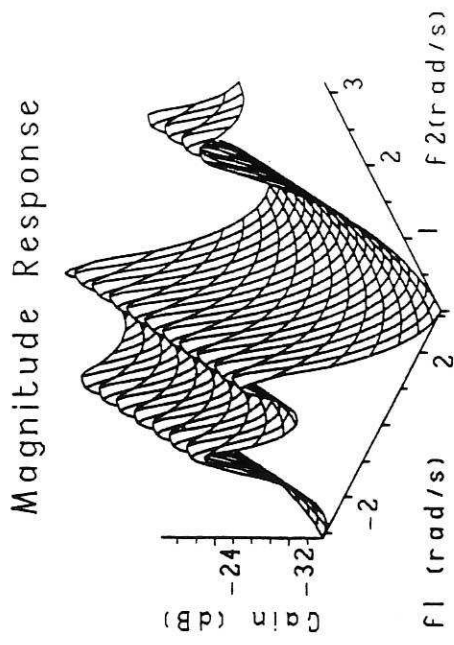


Fig 11. 2nd order response

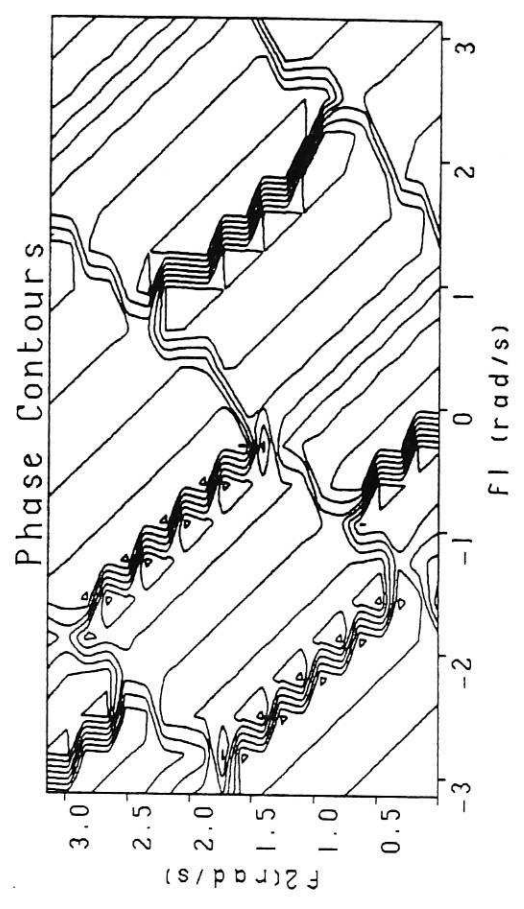
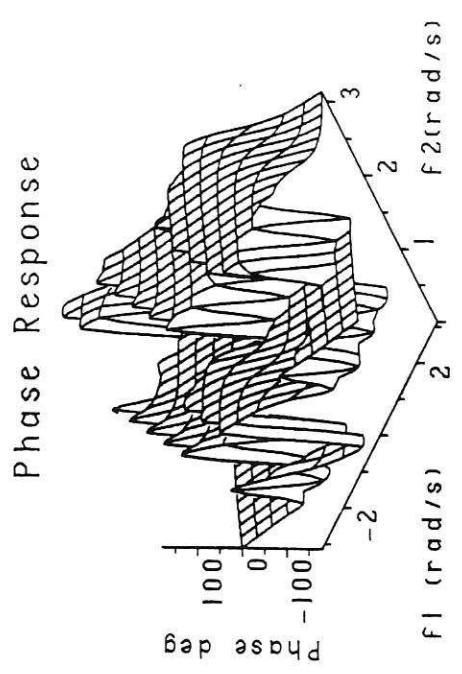
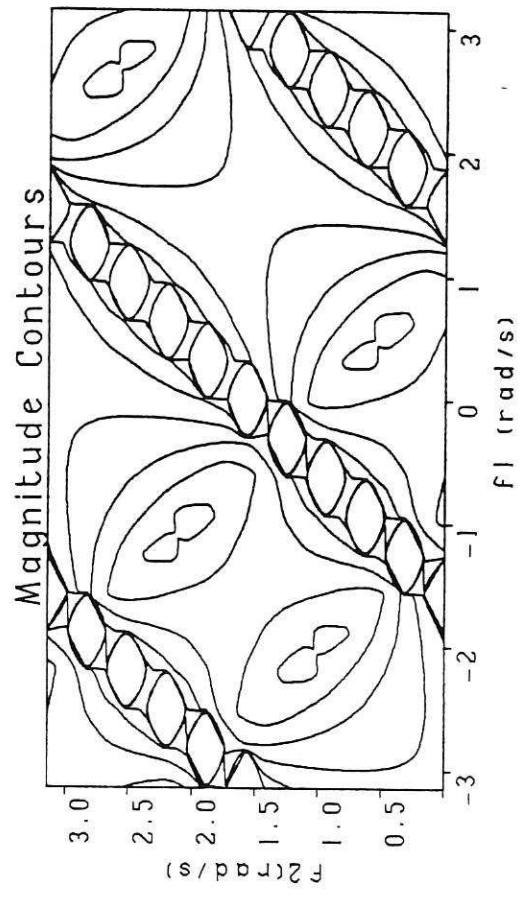
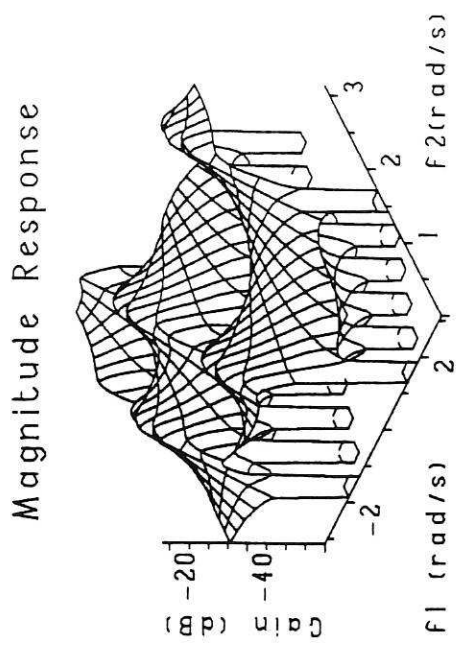


Fig 12. 2nd order response

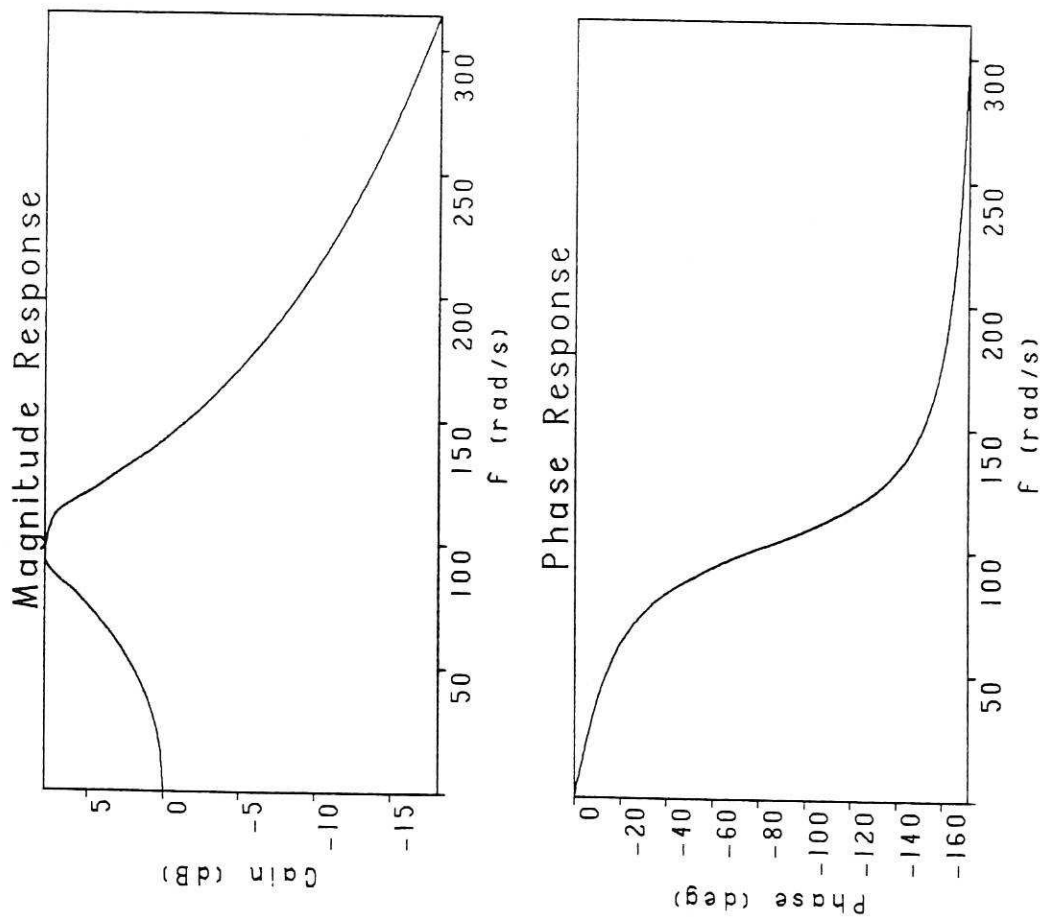
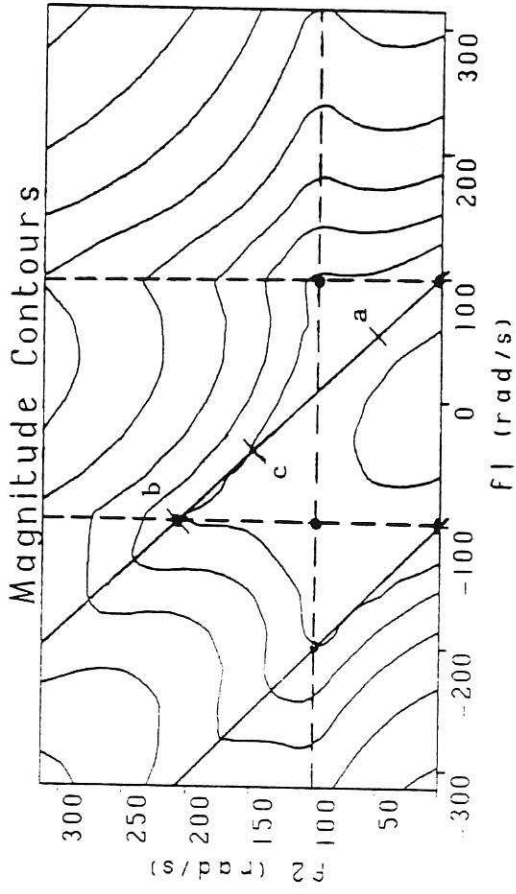
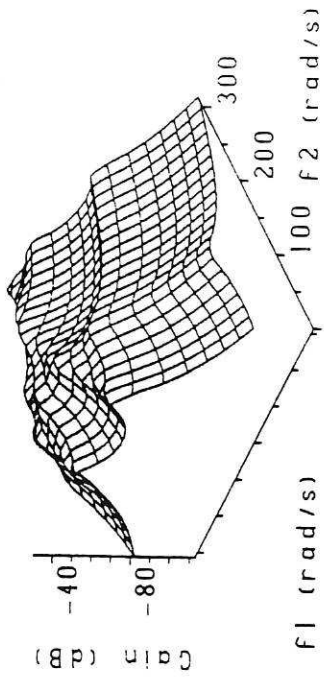


Fig 13. Linear response

Magnitude Response



Phase Response

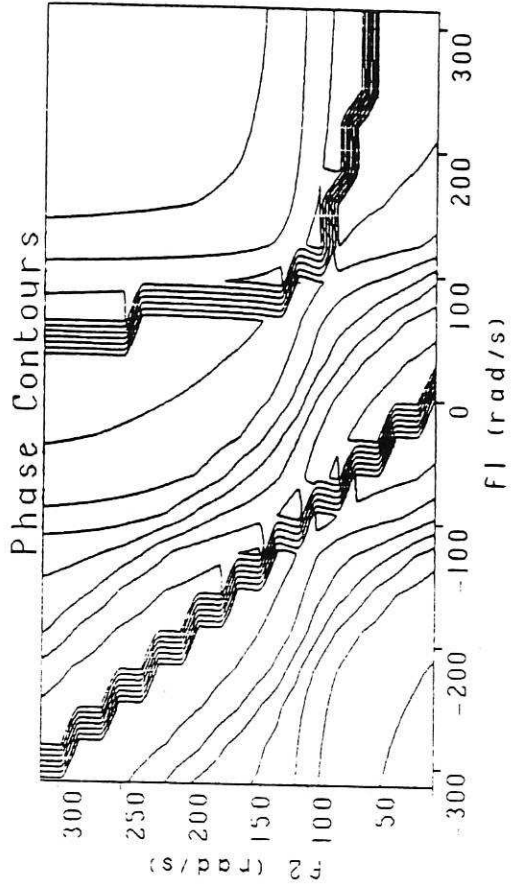
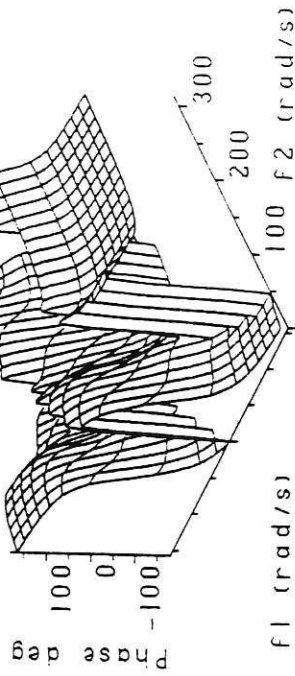


Fig 14. 2nd order response

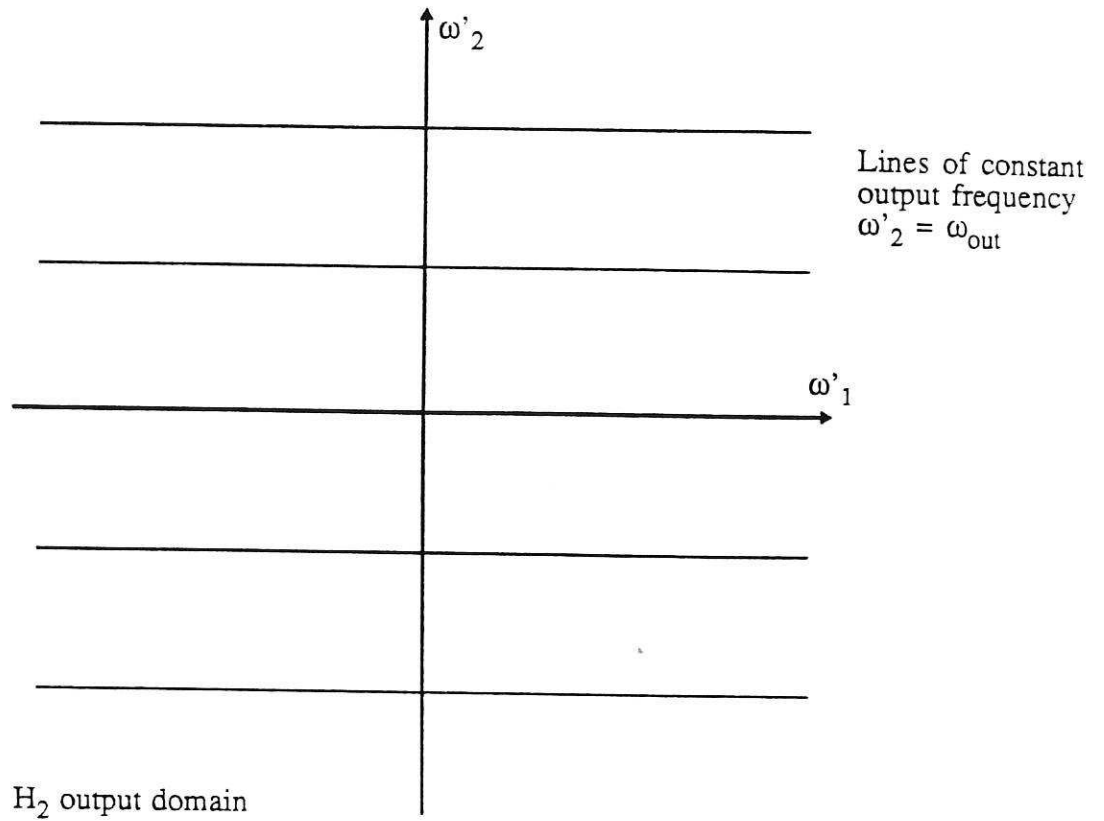


Fig 15 Constant output frequency sub-domains

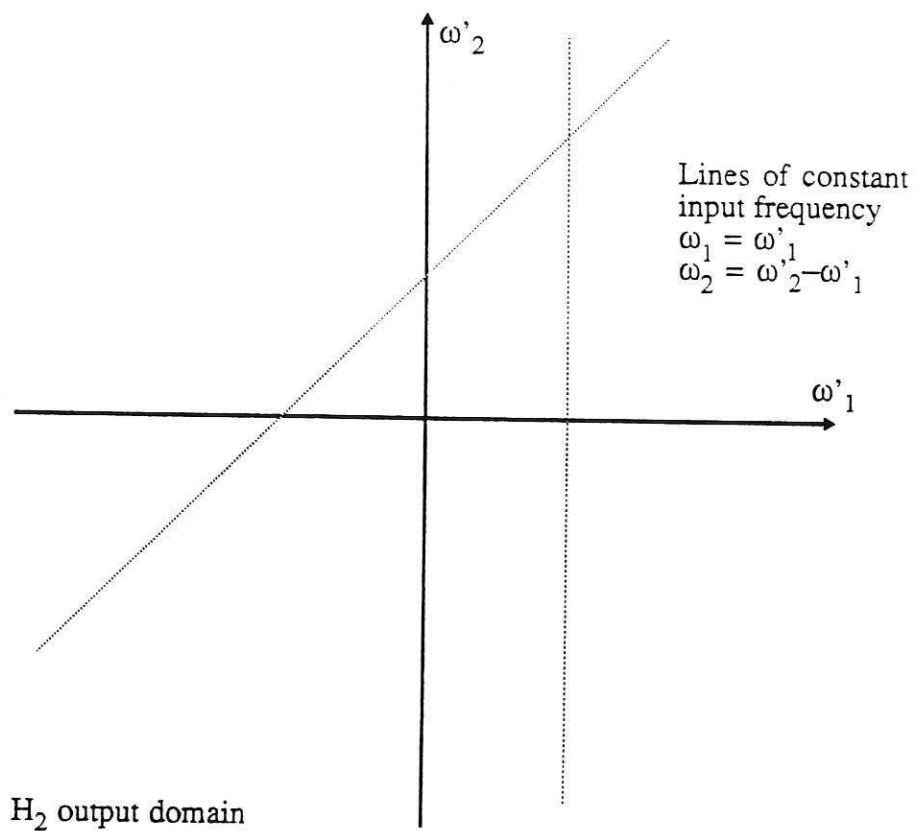


Fig 16 Constant input frequency sub-domains

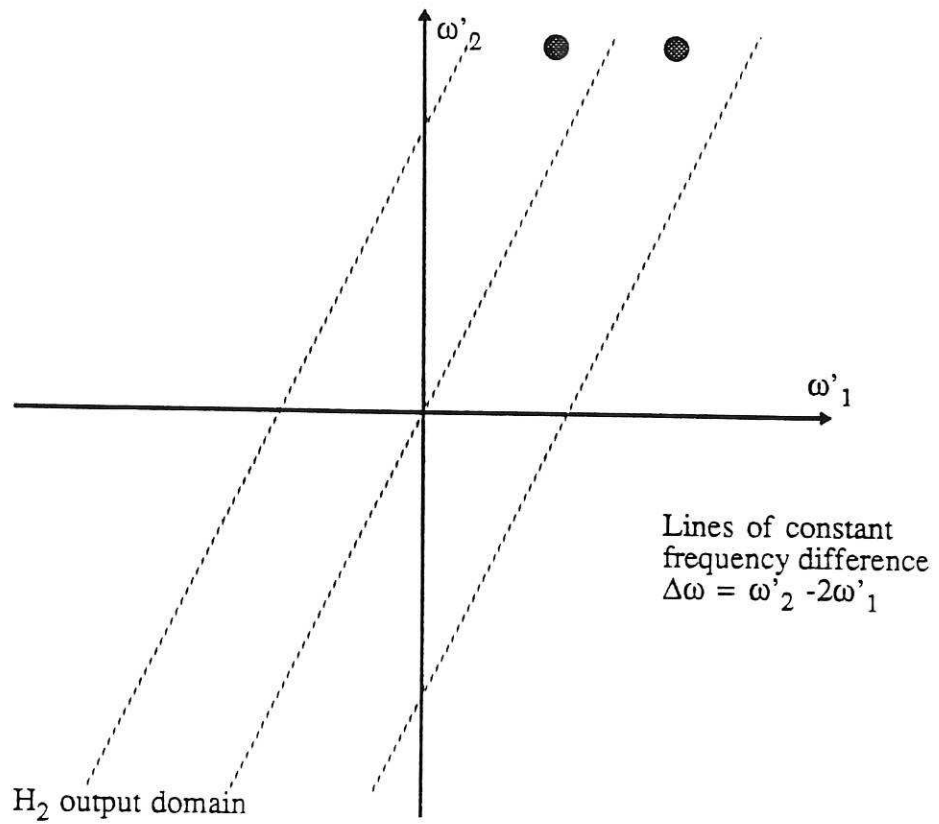


Fig 17 Constant difference frequency sub-domains

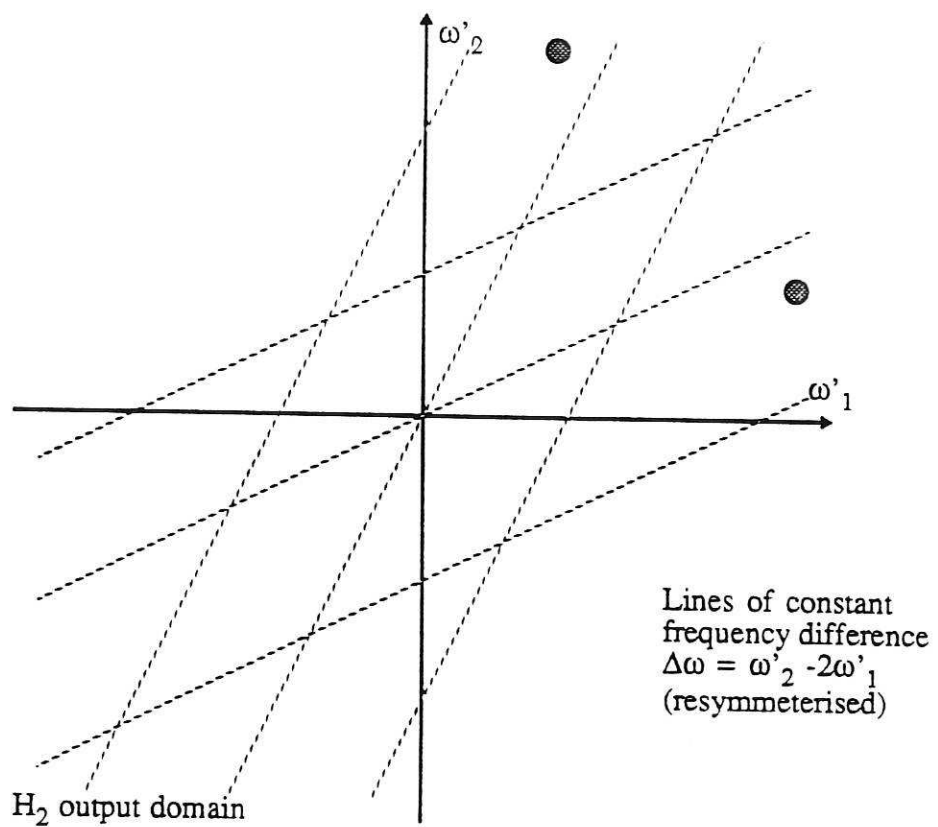


Fig 18 Constant difference frequency sub-domains (resymmetrised)

a: $H_2(j\omega_n/2, j\omega_n/2) = 20.7 \cdot 10^{-3} \angle 60^\circ$

b: $H_2(-j\omega_n, 2j\omega_n) = 10.0 \cdot 10^{-3} \angle 15^\circ$

c: $H_2(-j\omega_n/2, 3j\omega_n/2) = 11.6 \cdot 10^{-3} \angle -49^\circ$

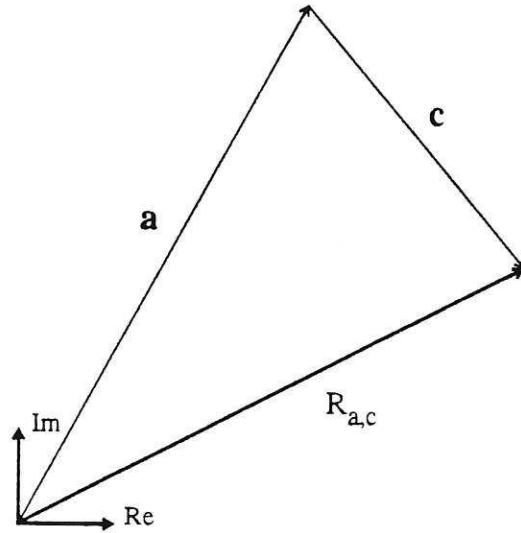
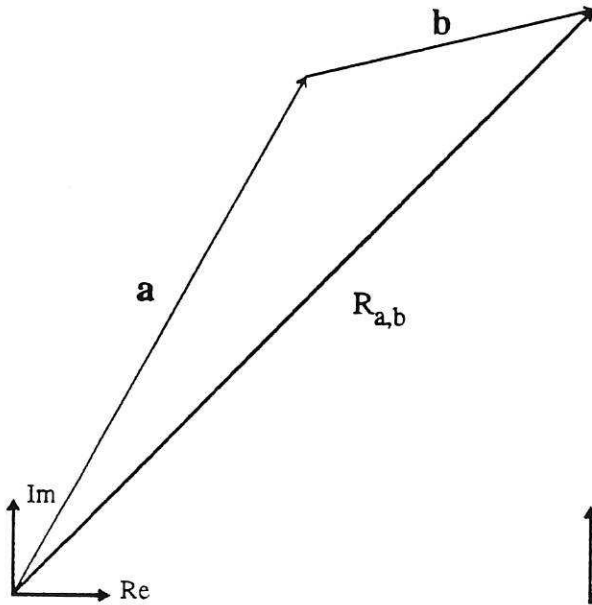


Fig 19 (a)

Constructive intra-kernel interference

Fig 19 (b)

Destructive intra-kernel interference

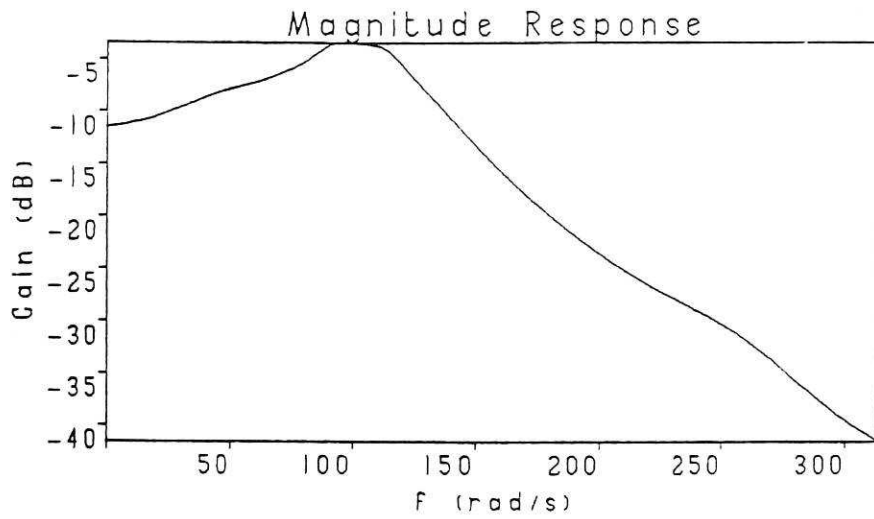


Fig 20 Worst case 2nd order output

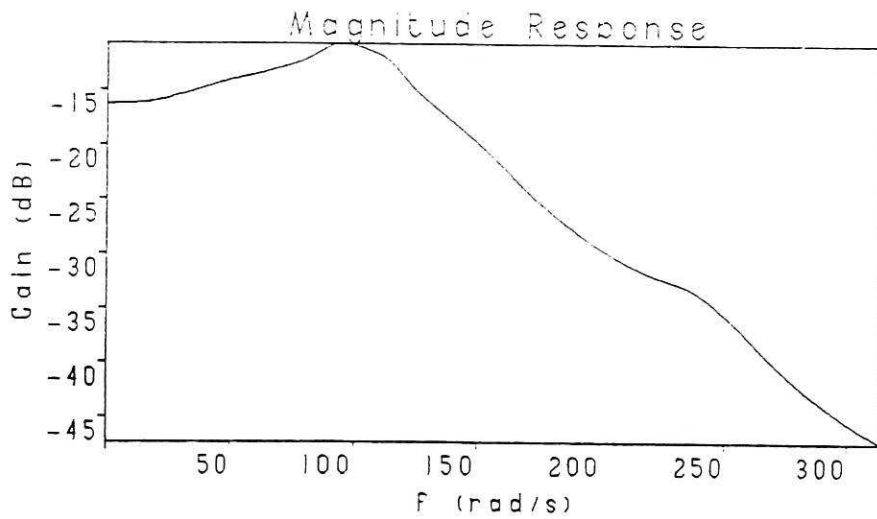


Fig 21 Worst case 3rd order output

$$\begin{aligned}
 Y_1(j\omega_a) &= 12.9 \cdot 10^{-3} \angle 75^\circ \\
 Y_2(j\omega_a) &= 6.7 \cdot 10^{-3} \angle 30^\circ \\
 Y_3(j\omega_a) &= 3.7 \cdot 10^{-3} \angle -116^\circ
 \end{aligned}$$

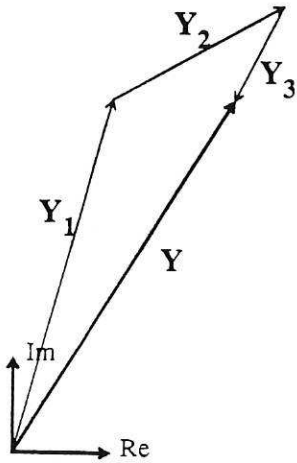


Fig 22 (a)
Gain expansion, phase retard

$$\begin{aligned}
 Y_1(j\omega_b) &= 16.4 \cdot 10^{-3} \angle 114^\circ \\
 Y_2(j\omega_b) &= 7.2 \cdot 10^{-3} \angle -125^\circ \\
 Y_3(j\omega_b) &= 2.6 \cdot 10^{-3} \angle 16^\circ
 \end{aligned}$$

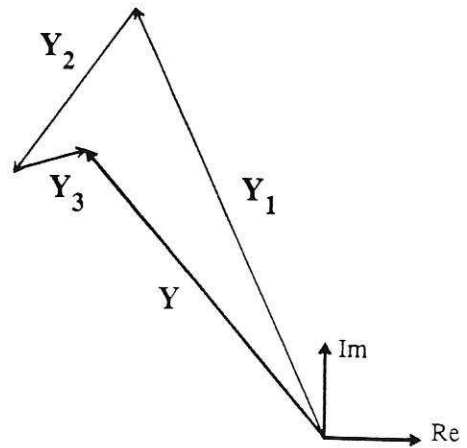


Fig 22 (b)
Gain compression, phase advance

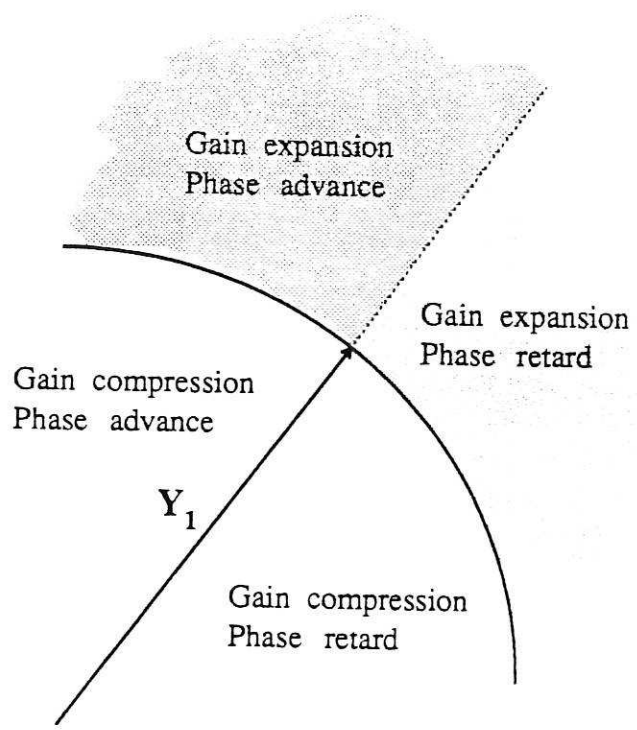


Fig 23 Regions of gain compression/expansion, and phase advance/retard

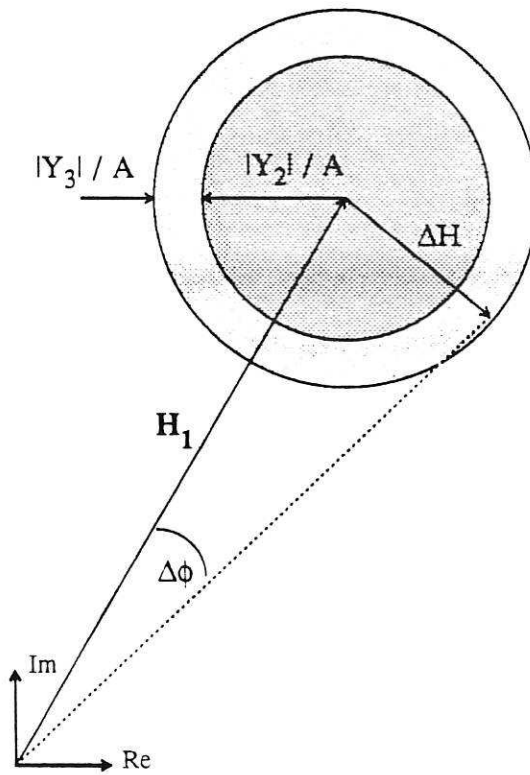


Fig 26 Worst case circles of uncertainty

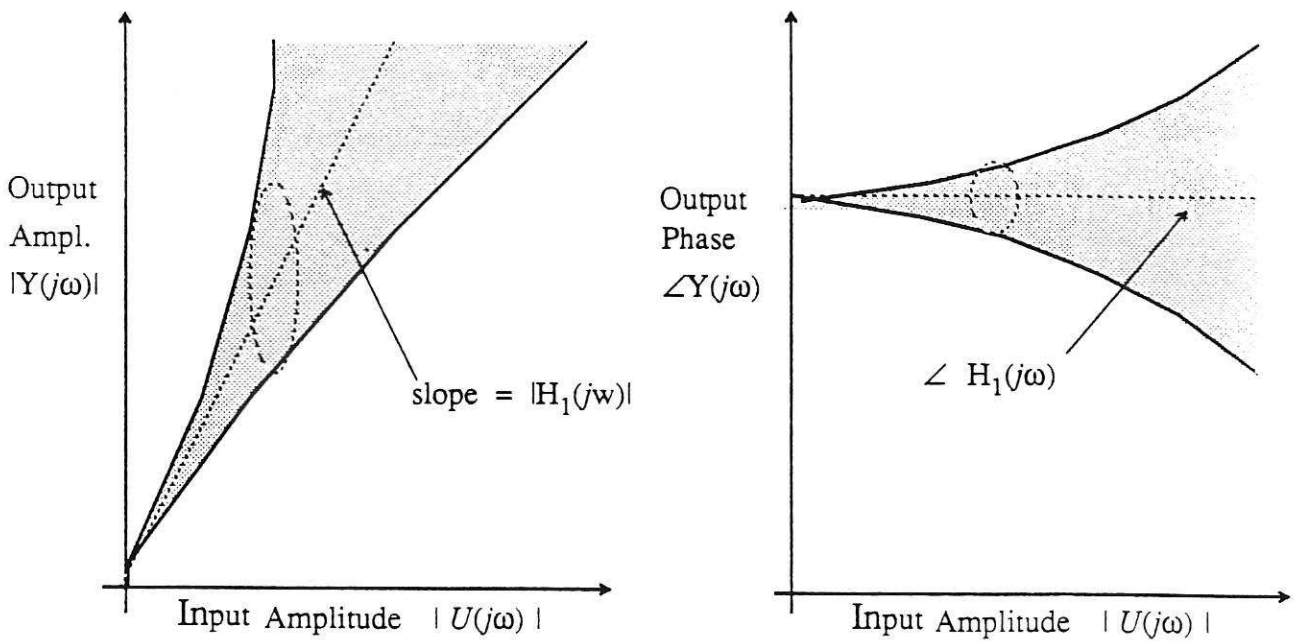


Fig 27 Worst case gain/phase response curves

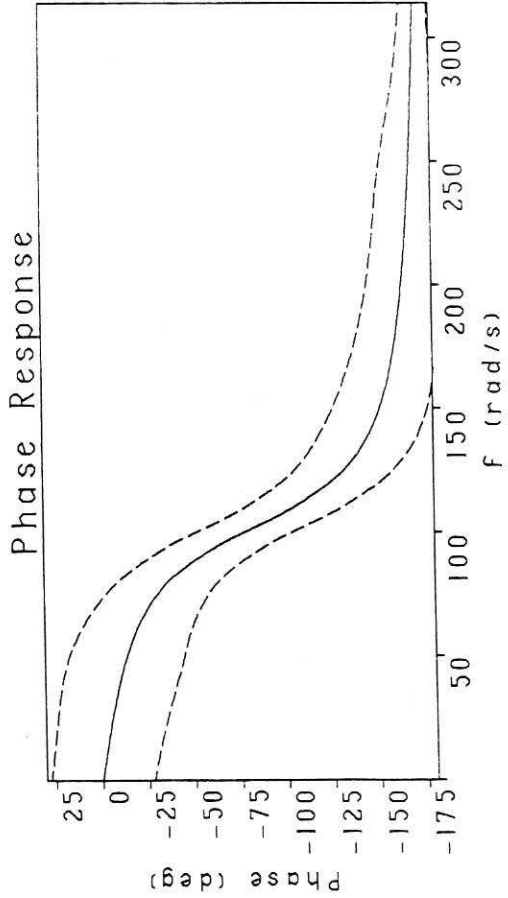
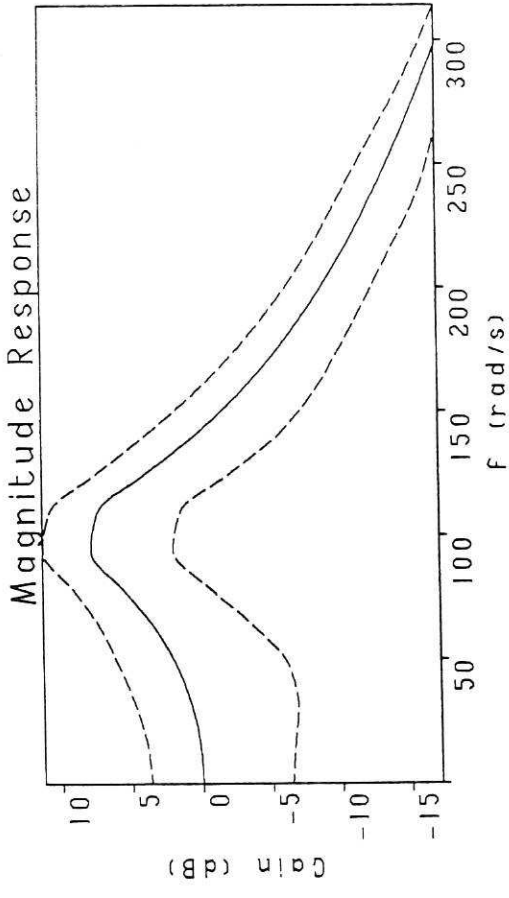


Fig 28 Worst case describing function

- Receivers Activities -

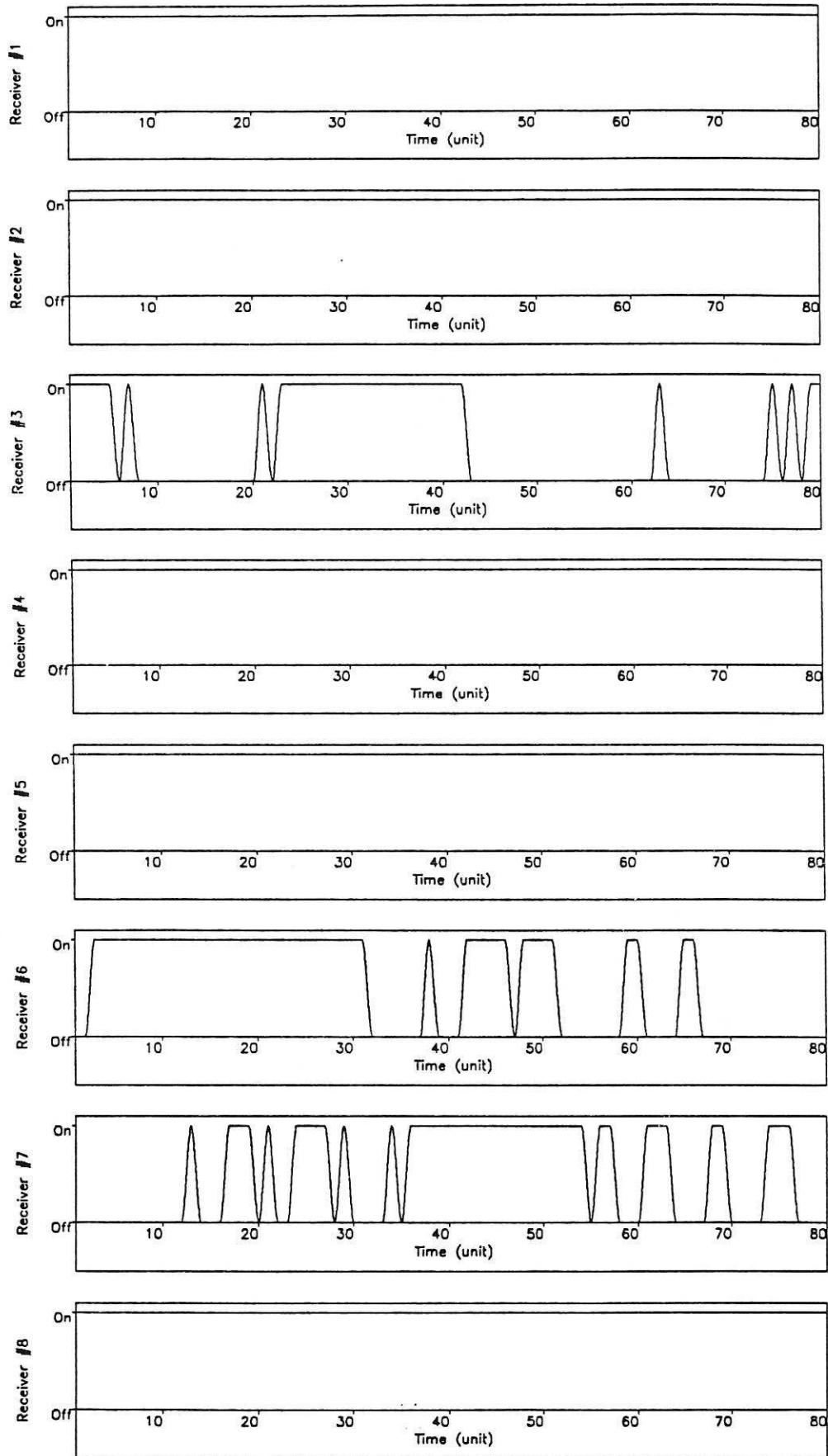


Figure (19)

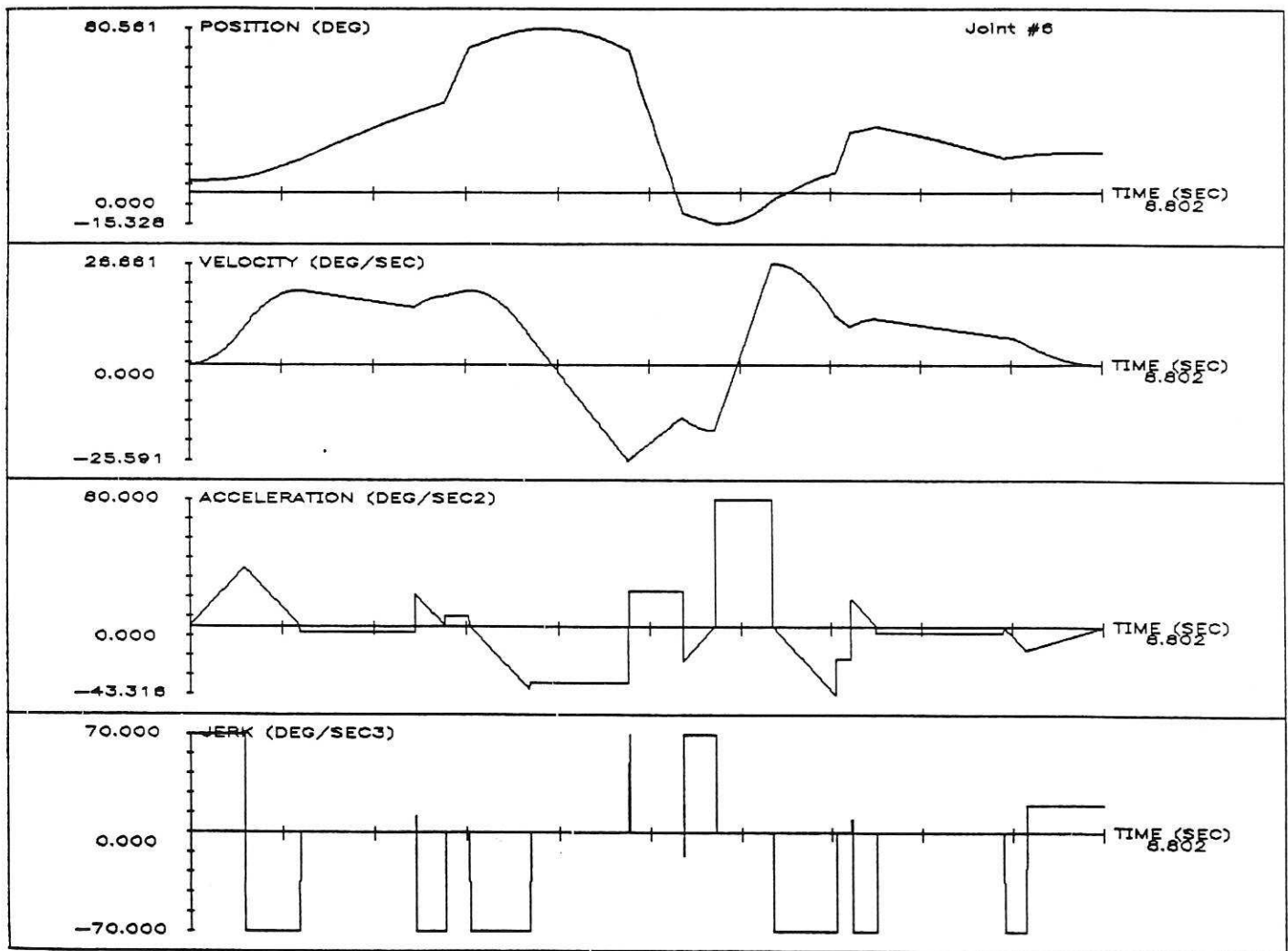


Figure 16